NASA TECHNICAL NOTE

NASA TN D-5729

AN EXPLORATORY WIND-TUNNEL INVESTIGATION OF THE WAKE EFFECT OF A PANEL TIP-MOUNTED FAN-JET ENGINE ON THE LIFT-INDUCED VORTEX

by James C. Patterson, Jr., and Stuart G. Flechner

Langley Research Center
Langley Station, Hampton, Va.

1. Report No. NASA TN D-5729	2. Government Accession No.	3. Recipient's Catalog No.	
4. Title and Subtitle AN EXPLORATORY WIND-TUNNEL INVESTIGATION OF THE WAKE EFFECT OF A PANEL TIP-MOUNTED FAN-JET ENGINE ON THE LIFT-INDUCED VORTEX		5. Report Date May 1970	
		6. Performing Organization Code	
7. Author(s) James C. Patterson, Jr., and Stuart G. Flechner		8. Performing Organization Report No. L-6898	
		10. Work Unit No. 737-01-10-01-23	
9. Performing Organization Name and Address NASA Langley Research Center Hampton, Va. 23365		11. Contract or Grant No.	
		13. Type of Report and Period Covered Technical Note	
12. Sponsoring Agency Name and Address National Aeronautics and Space Administration Washington, D.C. 20546			
		14. Sponsoring Agency Code	

15. Supplementary Notes

16. Abstract

An investigation has been conducted in the Langley 8-foot transonic pressure tunnel to determine the effectiveness of a tip-mounted powered-model high-bypass fan-jet engine in reducing the tip vorticity of an unswept symmetrical panel. The effects of end plates, a body of revolution, and a flow-through nacelle on panel-tip vorticity were also determined for comparison. All tests were conducted at a Mach number of 0.70, at angles of attack from approximately 0^0 to 4^0, and at a Reynolds number of 3.82×10^6 based on the mean geometric chord of 33.17 centimeters.

17. Key Words Suggested by Author(s) Fan-jet wake effect Drag due to lift Tip-vortex reduction	18. Distribution Statement Unclassified – Unlimited		
19. Security Classif. (of this report) Unclassified	20. Security Classif. (of this page) Unclassified	21. No. of Pages 41	22. Price* $3.00

*For sale by the Clearinghouse for Federal Scientific and Technical Information
Springfield, Virginia 22151

AN EXPLORATORY WIND-TUNNEL INVESTIGATION OF

THE WAKE EFFECT OF A PANEL TIP-MOUNTED FAN-JET ENGINE

ON THE LIFT-INDUCED VORTEX

By James C. Patterson, Jr., and Stuart G. Flechner
Langley Research Center

SUMMARY

An experimental wind-tunnel investigation has been conducted in the Langley 8-foot transonic pressure tunnel to determine the effectiveness of a powered-model high-bypass fan-jet engine, including engine wake, in reducing tip vorticity of an unswept symmetrical panel with the engine mounted on the panel tip. Tests were also performed with two end plates, a body of revolution, and a flow-through nacelle tip mounted on this panel. All tests were conducted at a Mach number of 0.70, at angles of attack from approximately 0° to 4°, and at a Reynolds number of 3.82×10^6 based on the mean geometric exposed chord of 33.17 centimeters.

The data indicate that tip vorticity and the associated drag due to lift may be reduced appreciably by the vortex canceling effect of the high-energy engine wake of the tip-mounted powered fan-jet engine. A similar but substantially less reduction may be obtained by a tip-mounted flow-through nacelle. A body of revolution similar in size to the flow-through nacelle, but with an elliptical nose and streamlined afterbody fairing tested here, is conducive to increased tip vorticity.

INTRODUCTION

A wind-tunnel investigation of the jet-wake effect of a high-bypass fan-jet engine on wing-pylon-nacelle interference for a logistic transport-type configuration has indicated that favorable interference can be obtained by properly orienting the engine and pylon relative to the wing (ref. 1). As noted in reference 1, this favorable effect was the result, in part, of the inboard end-plate action of the engine-pylon combination in reducing the induced drag of the configuration. It has been conjectured that the engine acts as an end plate on the pylon and that the engine wake tends to reduce the strength of the pylon tip vortex thereby allowing the pylon to become a more efficient inboard end plate. A more fundamental insight into such a possible phenomenon is required to understand more thoroughly and to maximize these favorable effects.

To explore more fully this possible phenomenon, an investigation has been conducted in the Langley 8-foot transonic pressure tunnel with a powered-model fan-jet engine mounted at the tip of an unswept, essentially untapered, symmetrical lifting panel. To provide a basis for comparison, tests were also made with end plates, a body of revolution, and a flow-through nacelle, each mounted on this same panel. All tests were conducted at a Mach number of 0.70, at angles of attack from approximately 0° to 4°, and at a Reynolds number of 3.82×10^6 based on the mean geometric exposed chord of 33.17 centimeters.

SYMBOLS

A	basic panel area, 0.7192 meter^2
AR	aspect ratio, $\dfrac{b^2}{A} = 6.18$
b	basic panel span, 210.8 centimeters
C_D	drag coefficient, $\dfrac{Drag}{qS}$
$\dfrac{\Delta C_D}{\Delta C_L{}^2}$	drag-due-to-lift factor
C_L	lift coefficient, $\dfrac{Lift}{qS}$
C_p	pressure coefficient, $\dfrac{p_l - p_\infty}{q}$
c	chord at panel pressure instrumentation station, 33.02 centimeters
l	length of body of revolution, 76.20 centimeters
M	free-stream Mach number
p_l	local static pressure, newtons/meter^2
p_∞	free-stream static pressure, newtons/meter^2
q	free-stream dynamic pressure, newtons/meter^2
S	exposed semispan reference area, 0.2847 meter^2

x   longitudinal distance, centimeters

α angle of attack, degrees

i   incidence angle, degrees

APPARATUS AND EXPERIMENTAL METHODS

Test Facility

This investigation was conducted in the Langley 8-foot transonic pressure tunnel which is capable of continuous operation through the subsonic, transonic, and low supersonic speed ranges. The test section of the wind tunnel has a slotted floor and ceiling with solid walls as shown in figure 1. The slots reduce the wall interference which allows tests of relatively large models at subsonic speeds. (See ref. 2.) The model used in the present investigation has a panel semispan equal to approximately 50 percent of the tunnel width and a balance fairing, panel, and powered-engine frontal area equal to 2.60 percent of the tunnel test-section cross-sectional area.

Model Configuration

A drawing of the semispan model used during this investigation is shown in figure 2. A photograph of the model with the engine mounted on the panel tip is shown in figure 3. Coordinates for each model component are given in table I.

Panel.- The unswept, essentially untapered panel, as shown in figure 2 has a chord of 33.02 centimeters over most of the span, an NACA 64_1A012 airfoil, and an aspect ratio of 6.18. To provide a path for the nitrogen used to drive the powered engine, it was necessary to increase the panel root chord. The exposed panel area, used as reference area for data reduction, includes the increase in area afforded by this extended root chord. The panel was constructed of steel and designed to accommodate the fan-jet engine, end plates, body of revolution, and flow-through nacelle at the panel tip in such a manner that the center line of each addition and the tip of the basic panel were at the same spanwise location. There is a small increase in panel area and aspect ratio resulting from the addition of the engine, body of revolution, and flow-through nacelle.

Balance fairing.- The wall-mounted force balance on which the basic panel was mounted protruded into the tunnel test section thereby requiring a fairing. This balance fairing has an elliptical nose, a cylindrical midsection where the panel is located, and a boattail afterbody.

Engine.- A cross-sectional view of the powered fan-jet engine used in this investigation is shown in figure 4. The two-stage fan is connected directly to a three-stage

turbine which is driven by compressed gaseous nitrogen that is piped through the test panel to the engine. The model simulates the output of an actual engine similar to that used on present large subsonic transports with a bypass ratio of 8 and a fan-exit total-pressure ratio of approximately 1.5 at the model-engine design maximum rotational speed of approximately 45 000 rpm.

The introduction of nitrogen into the wind-tunnel flow is considered to have little or no effect on the stream characteristics because of the similarity in the physical characteristics of nitrogen and air.

Flow-through nacelle.- The long duct flow-through nacelle shown in figure 2(b) was designed to have approximately the same maximum diameter and inlet area as the powered-engine fan cowl. The inlet internal diameter was maintained the entire length of the nacelle while the approximate external shape of the fan cowl was maintained up to the 20.5-percent nacelle station followed by a faired straight line, starting at the 24.6-percent station extending to the trailing edge of the nacelle simulating the fan-jet wake with a solid boundary.

Body of revolution.- The body of revolution shown in figure 2(b) had an elliptical nose, a cylindrical midsection with a diameter equal to that of the powered-engine fan cowl, and a boattail afterbody.

End plates.- The large end plate shown in figure 2(b) was designed to have the same shape as the profile of the body of revolution. It was 1.27 centimeters thick with semicircular edges having a radius equal to one-half the end-plate thickness.

The small end plate also shown in figure 2(b) had a straight leading and trailing edge, a chord equal to that of the panel tip, and height equal to the powered-engine fan-cowl diameter plus the additional height of fairings on the upper and lower ends of the end plate. These fairings were also semicircular in cross section with the local radius equal to one-half the local thickness of the end plate. The end plate was essentially a flat plate in cross section with a faired leading and trailing edge.

Each end plate was installed so that equal areas projected above and below the panel.

Instrumentation

Force balance.- Measurements of forces and moments were obtained from an internally mounted, wall-supported, five-component, electrical strain-gage balance. The model was designed so that the panel attached directly to the balance and protruded through a clearance opening in the balance fairing which was nonmetric. This fairing was attached to the balance wall-support system, but not to the balance, which allowed the fairing to traverse through the angle-of-attack range without the fairing forces being

measured by the balance. Since the balance fairing is cylindrical in the region of the panel, it is assumed that the interference effects are relatively small and are the same for each configuration tested.

Surface-pressure measurements.- Panel chordwise pressure measurements were made on the upper and lower surfaces at the 60- and 87-percent-semispan locations. Surface pressures were also measured on the upper surface of the body of revolution. Longitudinal locations of the pressure orifices are presented in table II.

Pressure rake.- Measurements of the wake velocity and wake direction were obtained at one and one-half engine lengths behind the 50-percent-panel-chord location with the yaw rake shown in figure 5. This rake consisted of nine total-head claws and eight static probes. Each claw consisted of five total-head tubes, two in the vertical plane, one inclined downward at 45° relative to the rake center line and the other inclined upward at this same angle, two tubes in the horizontal plane, also inclined toward each other in this plane with the same included angle of 90°, and one straight tube in the center to measure the local total pressure. This probe angle of inclination was chosen on the basis of data presented in reference 3 plus construction considerations.

Engine internal measurements.- The total and static pressures and total temperature were measured in the fan inlet and exit and in the turbine inlet and exit. These measurements were used to compute thrust.

The fan-inlet stagnation pressure was measured by four total-pressure rakes located just forward of the first-stage fan rotor at the 11°, 148°, 180°, and 240° circumferential locations. (See fig. 4.) In addition to the pressure measurements obtained by the six probes on each rake, an assumption that free-stream total pressure exists midway between the innermost rake probe and the fan hub was also used in the thrust computation.

Five static-pressure orifices were located on the fan-cowl inner surface at the 0°, 90°, 164°, 210°, and 270° circumferential positions and two static-pressure rakes were located circumferentially at the 128° and 350° positions. The static-pressure-rake support strut had a symmetrical airfoil section, 12° leading-edge sweep, and a 1.767-centimeter mean chord. The static-pressure orifice on each of the three probes on each static-pressure rake was located 1.016 centimeters behind the strut trailing edge to allow the flow to return to free-stream conditions before the static-pressure measurement was made.

There were seven total-head rakes at the fan exit located circumferentially at the 27°, 78°, 129°, 183°, 231°, 282°, and 333° positions. Each total-pressure rake had five probes spaced radially such that each probe was centered in one of five concentric circular equal area segments. These areas were then equally divided circumferentially among

the seven rakes thereby resulting in an equal weighing factor for each probe. A thermocouple probe was installed on each of the fan-exit total-head rakes, located radially at a position approximately equidistant from the inner fan cowl and the outer turbine cowl surfaces.

Just inside the fan exit, on the inner side of the cowl and on the turbine surface, static-pressure orifices were located at the 30°, 90°, 180°, 270°, and 330° positions. A linear static-pressure distribution from one surface to the other was assumed.

The turbine inlet-flow conditions were obtained from a turbine-type flow meter placed in the nitrogen supply line just prior to its entrance into the model. From measurements of the flow-meter turbine speed, the nitrogen pressure and temperature, and the meter volumetric flow calibration, the turbine inlet-flow conditions were established. The turbine-type meter is very susceptible to damage as a result of excessive or sudden load changes that may possibly alter the flow-meter turbine-blade pitch angle. To guard against this possibility the flow meter was recalibrated at the termination of the tunnel test. This calibration validated the pretest calibration.

The flow conditions existing at the turbine exit were obtained in a manner similar to that used at the fan exit with three total-head rakes located at the 60°, 183°, and 300° positions, and static-pressure orifices at the 90°, 180°, and 270° positions. Two thermocouple probes, at the 165° and 235° positions, were located upstream of the total-head rakes.

Calibration of model engine.- Because of the inadequacy of the flow-survey instrumentation in the fan inlet and exit, a calibration was required. The ASME flow nozzle used in reference 1 was used for this purpose where the actual engine-mass-flow rate could be determined through static measurements in the straight portion of the nozzle, the ambient stagnation pressure and temperature, plus the nozzle-flow coefficient of 0.992. This value was then ratioed to the mass-flow rate calculated from the fan-inlet measurements and the resulting flow coefficient was used to correct the inlet mass-flow rate measurements made during the investigation.

DATA REDUCTION

Force Data

The data for each configuration shown in figures 6 and 7 are measured results with no correction applied with the exception of the powered-engine configuration.

The drag data obtained from the force balance for the powered-engine configuration have been adjusted for engine thrust, calculated by the method described in reference 1,

and the lift and drag have also been adjusted for the change in engine thrust due to incidence of the engine.

No correction has been made for the incremental skin-friction drag, referred to as scrubbing drag, on the engine outer surface because of the change in local flow conditions caused by the addition of the powered flow, and in the case of the flow-through nacelle, the drag has not been corrected for internal drag. In both cases these corrections are essentially the same for all lift conditions which would not affect the incremental drag results discussed herein.

Drag Due to Lift

The drag-due-to-lift results shown in figure 8 are obtained from the difference in drag at lifting conditions and the drag at zero lift divided by the squared lift coefficient. For configurations involving incidence of the panel-tip configurations, the change in drag is obtained from the difference in the drag at lifting conditions for the various nacelle or engine incidences and the minimum drag for the 0° incidence configuration.

Vortex Measurements

The projected vortex velocity direction and magnitude were obtained by the yaw rake (see fig. 5) which was located one and one-half engine lengths downstream of the 50-percent-panel-chord location. The local velocity and local dynamic pressure at the rake location at the nine vertical probe positions were obtained from the total- and static-pressure rake measurements. The vertical and lateral directions of the local flow were determined from the yaw-rake differential pressure measurements in the vertical and lateral planes ratioed to the local dynamic pressure and the rake calibration which relates these rake differential pressure coefficients to local angle of attack. The resultant of these velocity vectors was then trigonometrically projected on to the vertical plane.

ACCURACY

The accuracy of the data, based on the balance calibrations and repeatability of the test data, is estimated to be within the following limits:

C_L . . . . ±0.01
C_D . . . . ±0.0003
α . . . . ±0.05
M . . . . ±0.002

The vortex velocity and flow direction obtained by the yaw rake for the basic wing, large end plate, body of revolution, and flow-through nacelle are considered accurate,

based on repeatability, within 2 feet per second and 10°. In the powered-engine case, however, the shock interference at the rake, as a result of the higher local Mach numbers due to the engine flow and the pronounced mixing in the wake, invalidates these data and therefore are not presented.

TEST CONDITIONS

Investigations were made of the basic panel, with the powered fan-jet engine mounted on the tip of the panel at incidence angles of 0° and -4°, with end plates, a body of revolution, and a flow-through nacelle mounted on the panel tip at incidence angles of 0°, -2°, and -4°.

All tests were conducted at a Mach number of 0.70 and over an angle-of-attack range of 0° to 4°. The Reynolds number based on the panel mean geometric exposed chord of 33.17 centimeters was 3.82×10^6.

The engine was operated at a fan-exit total-pressure ratio of 1.5 which was obtained at the design maximum engine speed of 45 000 rpm.

For all tests boundary-layer transition strips, 0.318 centimeter wide and consisting of No. 120 carborundum grains, were installed on the upper and lower surfaces of the panel at the 5.4-percent-chord location. Transition strips were also fixed on the engine and flow-through nacelles 1.27 centimeters behind the inlet leading edge both on the inside and outside of the inlet, 3.81 centimeters behind the nose of the body of revolution and large end plates, and 1.78 centimeters behind the leading edge of the small end plate.

PRESENTATION OF RESULTS

The results of the present investigation are presented in the following order:

RESULTS AND DISCUSSION

The basic drag results obtained for the various test configurations are presented against lift coefficient in figure 6. The lift data are presented against angle of attack in figure 7. The drag due to lift of the various configurations tested is presented against angle of attack to assure that the balance-fairing induced effects are the same for each configuration. The drag due to lift of the basic panel, the end plates, and body of revolution is presented against angle of attack in figure 8 including the theoretical limit of drag-due-to-lift factor for fully developed leading-edge suction with an efficiency factor of 1. The increase in drag due to lift of the basic panel at the higher test angles of attack noted in figure 8 is a result of a small degree of panel flow separation. Analysis of these data will be restricted to an angle of attack of 3^0 where the highest lift coefficient is developed before this separation occurs.

Nonpowered Effect

Effect of end plates.- The drag-due-to-lift results of the basic panel are higher than the theoretical value shown as would be expected for the untwisted rectangular planform panel with an associated loading distribution differing from the ideal elliptical loading. There is a reduction in drag due to lift associated with both end-plate configurations tested, as would be expected.

9

The reduction in drag due to lift resulting from the addition of the large end plate to the basic panel is associated with an alteration in the panel downwash which manifests itself as an increase in panel leading-edge suction as shown in figure 9(a). The small end plate produced approximately the same pressure profile even though the drag due to lift is less for this configuration.

The wake-survey data shown in figure 11(a) indicate a reduction in tip vorticity associated with the large end plate compared with the basic panel. The wake was not measured behind the small end plate, but it is believed that the larger reduction in drag due to lift obtained for the small end-plate configuration is a result of the end-plate trailing-edge configuration. The main tip vortex is probably shed as two smaller vortices, one from the upper and one from the lower edge of the end plate, thereby reducing the strength of each vortex shed plus increasing the distance over which each vortex must act, together reducing their influence on the downwash behind the panel.

Effect of body of revolution.- An increase in drag due to lift resulting from the addition of the body of revolution to the basic panel is contrary to that anticipated. The unexpected adverse effect of the body of revolution on drag due to lift required a more detailed study of the test results. The panel pressures measured in the vicinity of the tip (fig. 9(a)) show an increase in lift in this region with the body of revolution present that is even greater than that provided by the end plates owing in part to the end-plate effect derived from the presence of the body of revolution and in part to the induced effects resulting from the lift on the body of revolution. However, the wake measurements obtained with the body of revolution, shown in figure 11(a), indicate a greater tip vorticity than that produced by the basic panel. Furthermore, pressures measured along the upper surface of the body at angles of attack of approximately 0° and 3°, presented in figure 10, indicate a large drop in pressure at the rear of the body at lifting conditions, probably as a result of the low pressure in the vortex being shed from the body. These results suggest that the increase in drag due to lift of the body of revolution results from the fact that it produces an increase in energy loss in the vortex as a result of the vortex concentrating effect of the body which is more important than the favorable end-plate effect derived from this configuration.

Effect of flow-through nacelle.- The drag-due-to-lift results for the flow-through nacelle are presented in figure 8(b) for nacelle incidences of 0°, -2°, and -4°. There is a reduction in drag due to lift in each case at an angle of attack of 3° compared with the drag due to lift of the basic panel. The lowest value of drag due to lift for this angle of attack is obtained by the -2° incidence case where the nacelle is more closely alined with local flow. This drag-due-to-lift value is approximately the same as that obtained by the small end plate. Setting the nacelle at either 0° or -4° incidence results in an additional

misalinement interference drag at 3° angle of attack, the increment increasing with angle of attack for the 0° incidence case, decreasing for the -4° incidence case as would be expected.

The panel pressures presented in figure 9(b) indicate an increase in panel leading-edge suction associated with the installation of the flow-through nacelle compared with the basic panel and the end-plate configurations. This increase suggests, as in the case of the body of revolution, that the presence of the nacelle alters the flow fields such that there is an increase in the effective angle of attack plus an additional induced effect of nacelle lift. Even though a somewhat greater lift is obtained for the 0° incidence case, the drag due to nacelle misalinement is less for the -2^O incidence case at 3° angle of attack thereby resulting in a lower drag due to lift for this configuration.

In addition to the induced flow over the panel, the wake-survey results shown in figure 11(b) indicate that the rotation of the vortex core is virtually eliminated for the -2^O incidence case. The canceling effect in this case possibly results from the fact that the flow passing through the nacelle is isolated from the influence of the tip vortex flow circumscribing the nacelle. The inner flow would then leave the nacelle as a nonrotating tube of air which retards the development of the tip vortex.

Powered Effect

Effect of jet wake.- The drag-due-to-lift results for the powered engine at 0° and -4° incidence are presented in figure 8(c). Here again as in the case of the flow-through nacelles there is a misalinement drag associated with both the 0° and -4° engine incidence which for the -4° incidence case is greater at the lower test angles and decreases with angle of attack as the engine becomes more alined with the local flow whereas the reverse is true for the 0° incidence case. These data indicate that a reduction in drag due to lift is obtained by the powered-engine configuration at an angle of attack of 3° and an incidence angle of 0° of approximately one-third the drag due to lift produced by the basic panel. This is more than twice the reduction obtained by the flow-through nacelle at the same angle of incidence. Based on the results obtained for the flow-through nacelle it might be concluded that an even greater reduction in drag due to lift may be obtained by the powered engine with an incidence angle of -2^O. This large reduction in drag due to lift is considered to be the result of a reduction in tip vorticity caused by the nonrotating engine wake being introduced into the flow at the panel tip. This is similar to the phenomenon that exists for the flow-through nacelle with an even greater restraint toward the tip vortex buildup offered by the high-energy engine flow which should more amply reduce the rotational speed of the vortex core. It might be expected that even a greater reduction in tip vorticity may be obtained by prerotating the engine-fan exhaust in a direction opposite to that of the vortex. This is shown to be true in reference 4 where

a tip-mounted propeller was tested with a provortex rotation in one case which increased the downwash behind the wing and a countervortex rotation in another case which reduced the downwash and the associated drag due to lift.

The panel pressures presented in figure 9(c) for the powered-engine case indicate an increase in leading-edge suction similar to that of the flow-through nacelle.

CONCLUSIONS

The results of an experimental investigation to determine the mechanism by which a tip-mounted powered-model high-bypass fan-jet engine may reduce the tip vorticity of an unswept symmetrical panel and the degree of its effectiveness relative to more conventional tip treatments indicate the following:

1. The drag due to lift may be reduced appreciably by the fan wake of a tip-mounted powered fan-jet engine. The results of this investigation suggest that part of the tip-vortex energy is dissipated by the nonrotating high-energy wake thereby resulting in a reduction in downwash behind the panel and the associated drag due to lift.

2. A tip-mounted flow-through nacelle experienced a vortex canceling effect similar to that of the powered engine but to a lesser degree. This effect is the result of a reduction in rotational speed of the vortex core, as indicated by the wake survey, as a result of the isolating effect offered by the nacelle to the flow passing through the nacelle.

3. A panel-tip configuration such as the body of revolution tested here may be conducive to increased tip vorticity by virtue of the vortex concentration effect of its shape resulting in an increase in drag due to lift associated with a very low pressure at the base of the body.

Langley Research Center,
        National Aeronautics and Space Administration,
                Langley Station, Hampton, Va., January 16, 1970.

REFERENCES

1. Patterson, James C., Jr.: A Wind-Tunnel Investigation of Jet-Wake Effect of a High-Bypass Engine on Wing-Nacelle Interference Drag of a Subsonic Transport. NACA TN D-4693, 1968.

2. Wright, Ray H.; Ritchie, Virgil S.; and Pearson, Albin O.: Characteristics of the Langley 8-Foot Transonic Tunnel With Slotted Test Section. NACA Rep. 1389, 1958. (Supersedes NACA RM L51H10 by Wright and Ritchie and RM L51K14 by Ritchie and Pearson.)

3. Schulze, Wallace M.; Ashby, George C., Jr.; and Erwin, John R.: Several Combination Probes for Surveying Static and Total Pressure and Flow Direction. NACA TN 2830, 1952.

4. Synder, Melvin H., Jr.: Effects of a Wingtip-Mounted Propeller on Wing Lift, Induced Drag, and Shed Vortex Pattern. Ph. D. Thesis, Oklahoma State Univ., May 1967.

TABLE I.- MODEL COORDINATES

(a) Fan-jet-engine coordinates

[Stations and radii in percent length]

Station	Radius
Fan cowl	
0	13.96
.4	14.40
1.6	14.81
3.6	15.22
6.3	15.63
12.3	16.01
19.8	16.01
30.2	15.84
34.9	15.49
37.7	15.13
39.7	14.94
Turbine cowl	
39.7	10.52
44.8	10.35
51.1	10.00
57.0	9.64
62.0	9.26
67.1	8.88
71.3	8.47
75.5	8.03
79.7	7.57
81.9	7.33
Plug	
81.9	4.73
84.9	4.48
88.7	3.96
92.0	3.33
94.9	2.60
98.5	1.50
100.0	0

TABLE I.- MODEL COORDINATES – Continued

(b) Body-of-revolution and large end-plate coordinates

[Stations, radii, and ordinates in percent length]

Station	Radius (body of revolution)	Ordinate (large end plate)
0	0	0
.3	1.47	1.47
.7	2.07	2.07
1.0	2.53	2.53
1.3	2.90	2.90
1.7	3.23	3.23
3.3	4.53	4.53
6.7	6.20	6.20
10.0	7.33	7.33
13.3	8.20	8.20
16.7	8.80	8.80
20.0	9.27	9.27
23.3	9.57	9.57
29.3	9.77	9.77
51.0	9.77	9.77
53.2	9.73	9.73
55.5	9.67	9.67
59.9	9.47	9.47
64.4	9.07	9.07
68.8	8.53	8.53
73.2	7.83	7.83
77.6	6.97	6.97
81.9	5.97	5.97
86.2	4.80	4.80
90.5	3.50	3.50
94.7	2.07	2.07
98.9	.47	.47
100.0	0	0

TABLE I.- MODEL COORDINATES — Continued

(c) Small end-plate coordinates

[Stations and ordinates in percent length]

Station	Ordinate
0	0
.4	.46
.8	.69
1.2	.92
1.9	1.15
2.7	1.31
3.8	1.54
5.8	1.69
7.7	1.85
9.6	1.92
84.6	1.92
88.5	1.69
92.3	1.23
96.2	.69
100.0	0

TABLE I.- MODEL COORDINATES – Continued

(d) Flow-through-nacelle coordinates

[Stations and radii in percent length]

Station	Radius
Inside contour	
0	14.41
.3	13.99
.5	13.83
.8	13.72
1.1	13.61
1.4	13.55
1.6	13.50
1.9	13.44
2.2	13.42
2.7	13.39
4.1	13.33
5.5	13.30
100.0	13.30
Outside contour	
0	14.41
.3	14.75
.5	14.92
.8	15.03
1.1	15.14
1.6	15.30
2.2	15.51
2.7	15.46
3.8	15.57
5.5	15.74
8.2	15.85
10.9	15.97
20.5	15.97
21.9	15.90
24.6	15.85
100.0	13.43

TABLE I.- MODEL COORDINATES — Concluded

(e) Balance-fairing coordinates

[Stations and ordinates in percent length]

Station	Ordinate
0	0
.4	1.4
.8	2.0
1.2	2.4
1.6	2.8
2.0	3.1
2.4	3.4
2.8	3.6
3.2	3.9
6.3	5.1
7.9	5.5
9.5	5.8
11.1	6.0
12.7	6.1
14.3	6.2
65.9	6.2
68.3	6.1
70.2	6.1
72.2	6.0
74.2	5.8
76.2	5.6
78.2	5.3
80.2	5.0
82.1	4.7
84.2	4.3
88.1	3.4
100.0	.5

TABLE II.- LONGITUDINAL LOCATIONS OF PRESSURE ORIFICES

[Stations in percent local longitudinal length]

Basic panel	Body of revolution
1.0	3.33
2.5	6.67
5.0	10.00
7.5	13.33
10.0	16.67
20.0	20.00
30.0	23.33
40.0	26.67
50.0	30.00
65.0	33.33
85.0	36.67
100.0	40.00
	43.33
	46.67
	50.00
	53.33
	56.67
	60.00
	63.33
	66.67
	70.00
	73.33
	76.67
	80.00
	83.33
	86.67
	90.00
	93.33
	96.67
	100.00
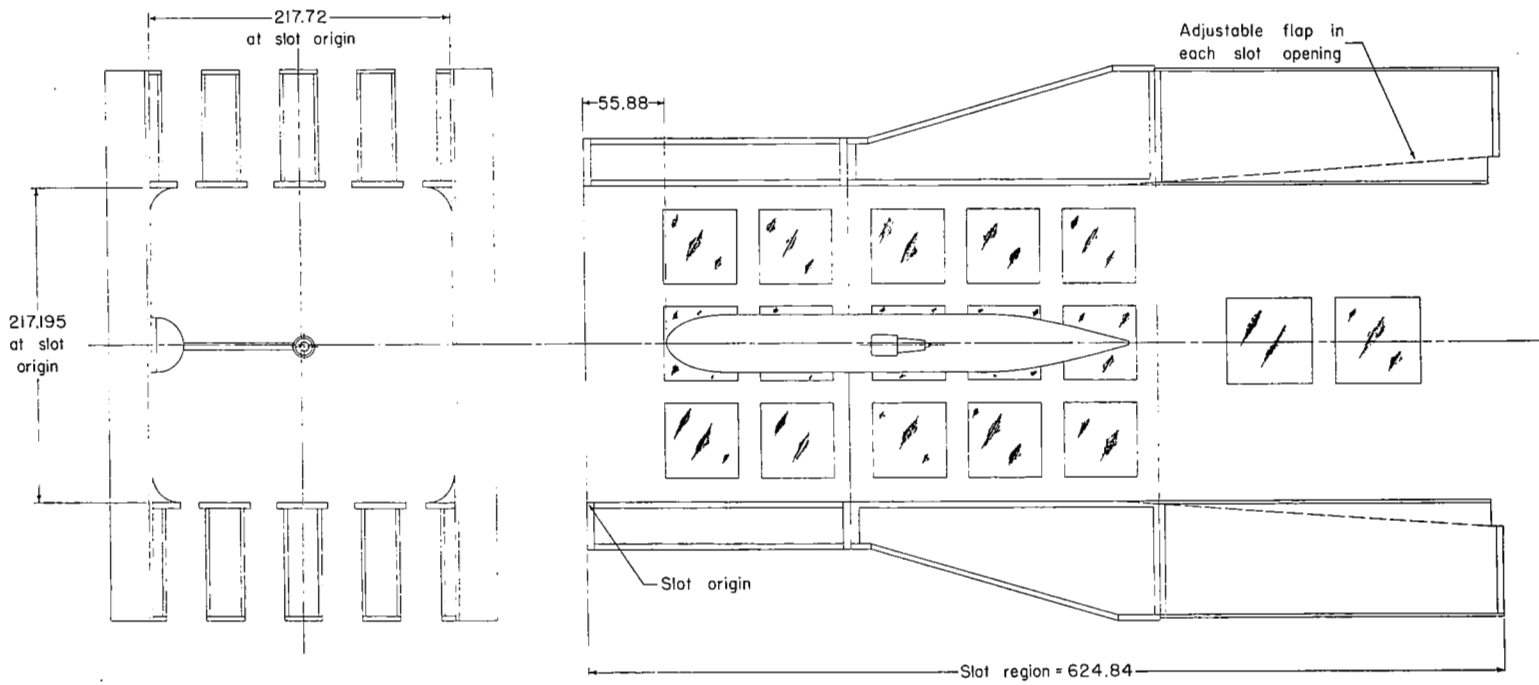
Figure 1.- Details of test section and location of model in Langley 8-foot transonic pressure tunnel. All dimensions are in centimeters.

5.08 spacer

28.85

15°

105.41

c/4

Diam = 14.88

150.34

33.02

Basic panel
with tip

166.85

Balance center

.58

Diam = 39.37

140.16

46.49

320.04
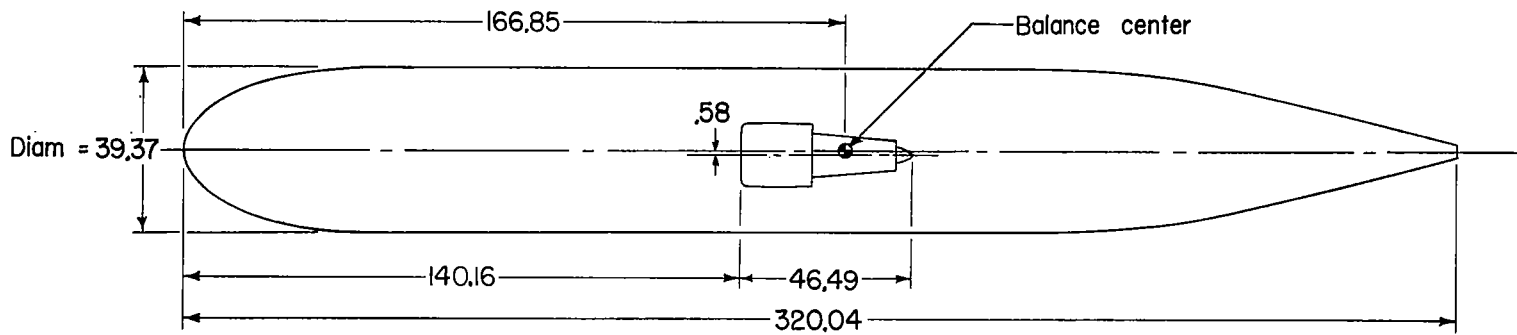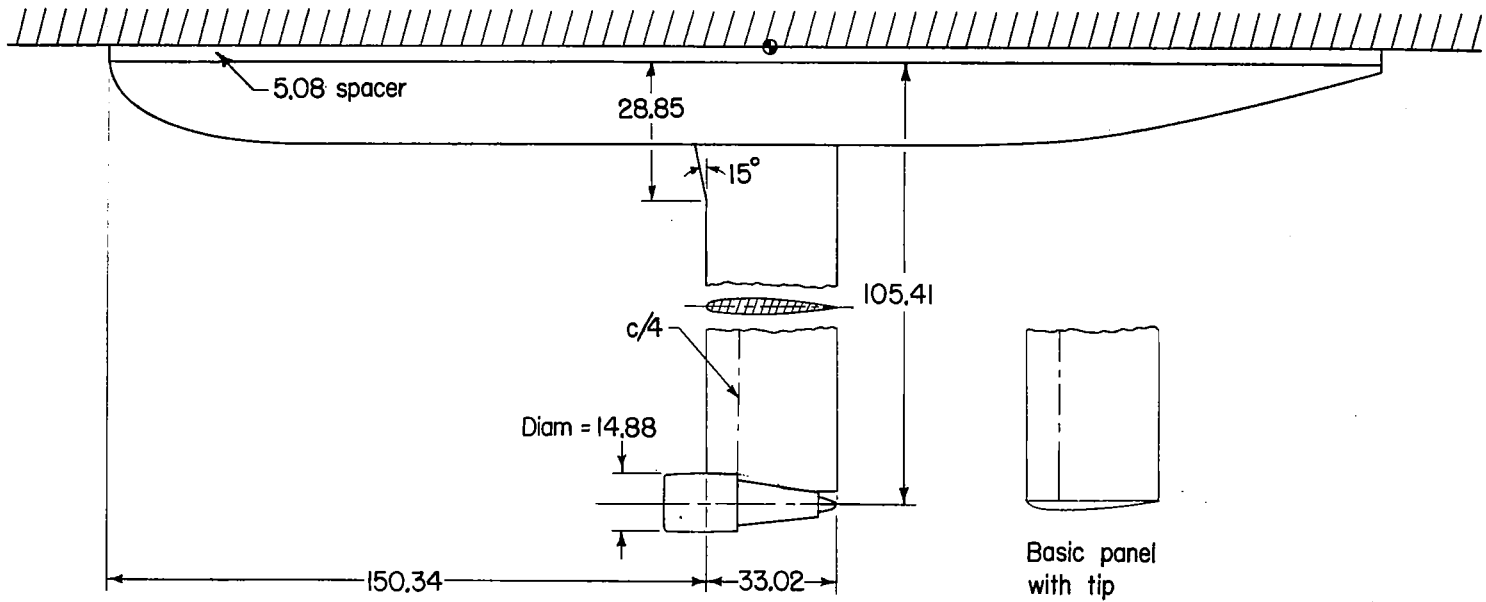
(a) Details of test model.

Figure 2.- Drawing of semispan model. All dimensions are in centimeters.

76.20

14.88

17.42

22.35

1.27

1.27
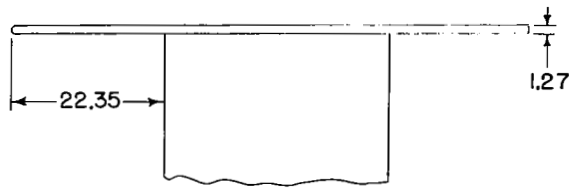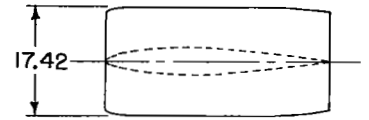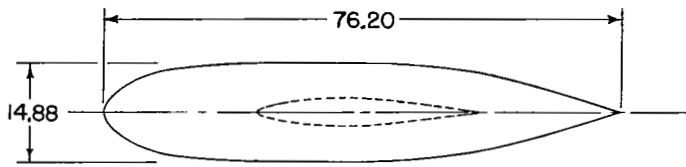
Large end plate

Small end plate

76.20

46.48

Diam = 14.88

Diam = 14.88

22.35

10.21
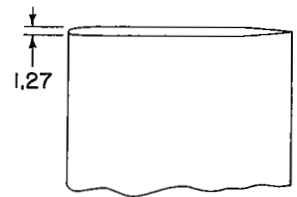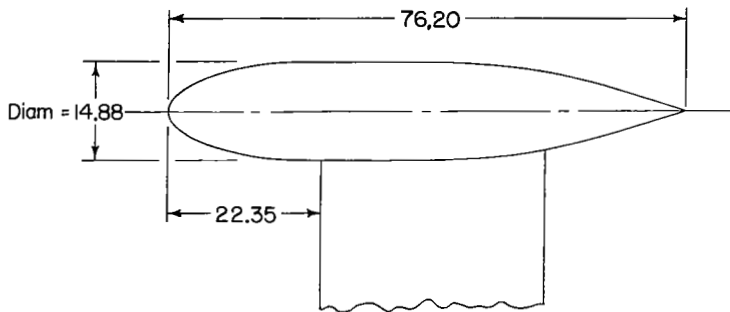
Body of revolution
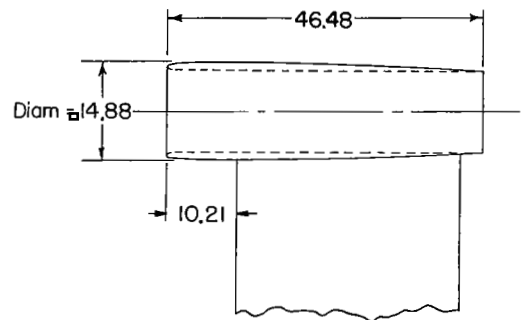
Flow-through nacelle

(b) Details of tip configurations.

Figure 2.- Continued.

Cowl   Turbine   Plug
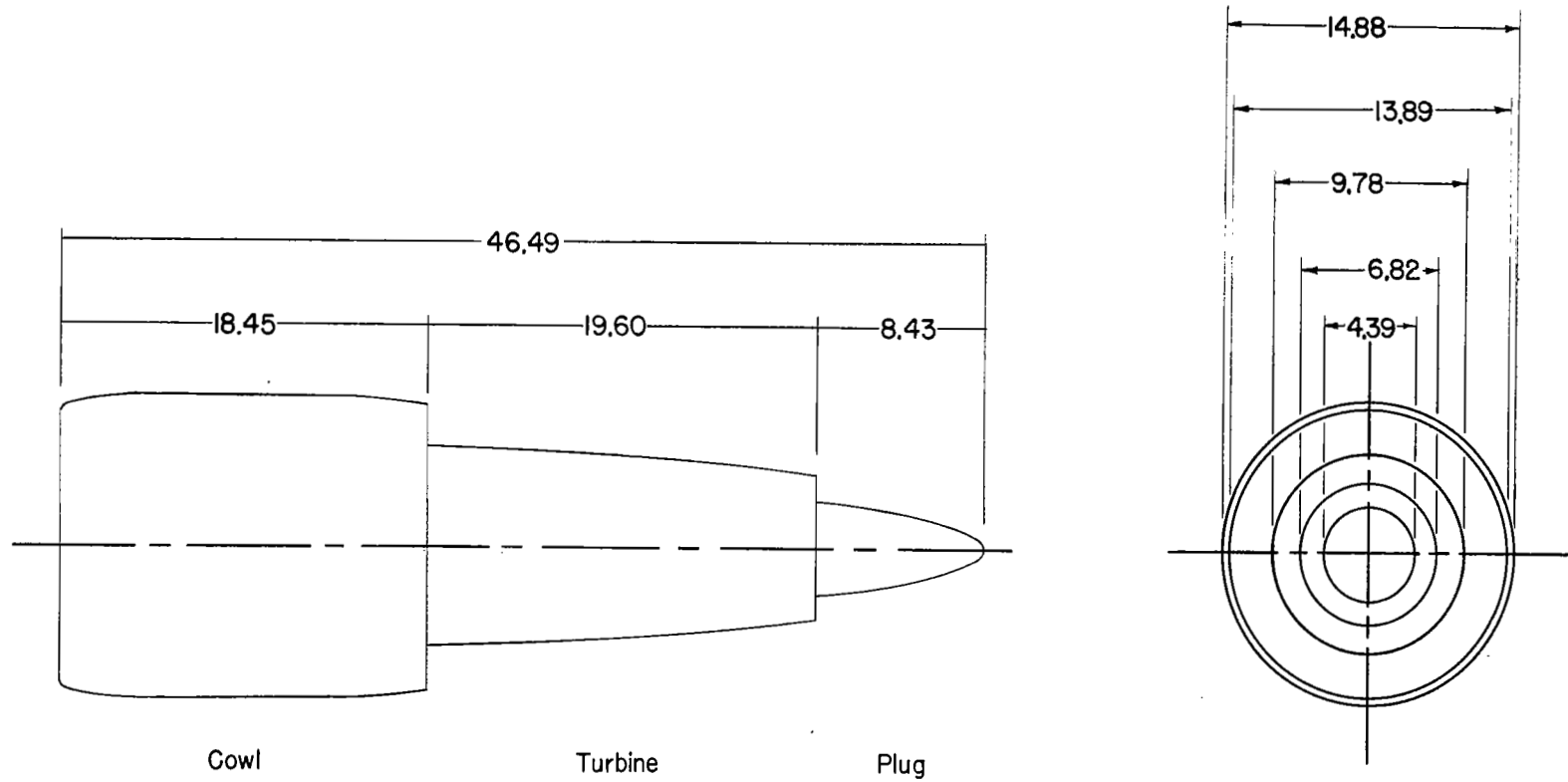
(c) Details of model engine.

Figure 2.- Concluded.
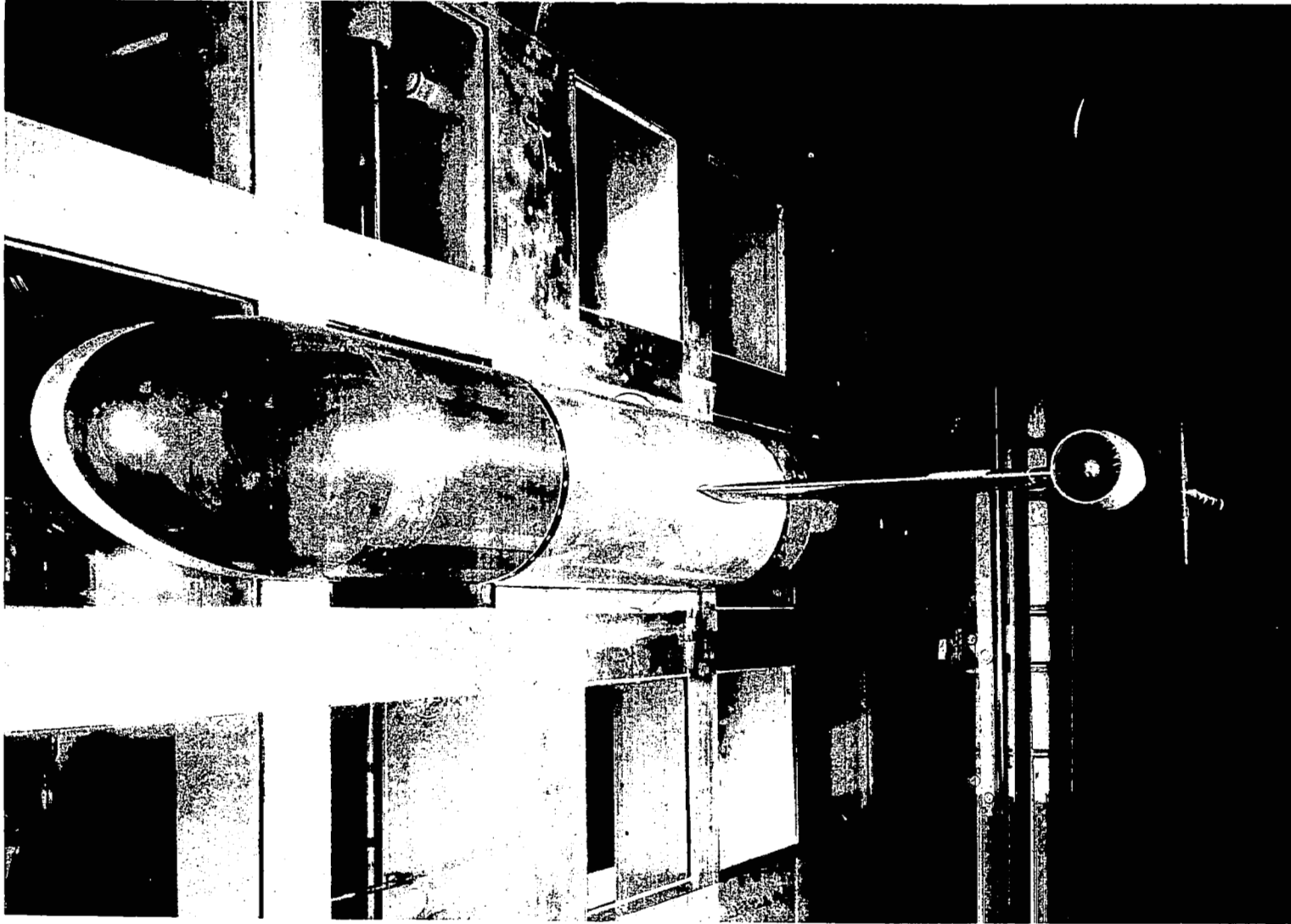
Figure 3.- Photograph of semispan model wall mounted in Langley 8-foot transonic pressure tunnel.

L-68-3002
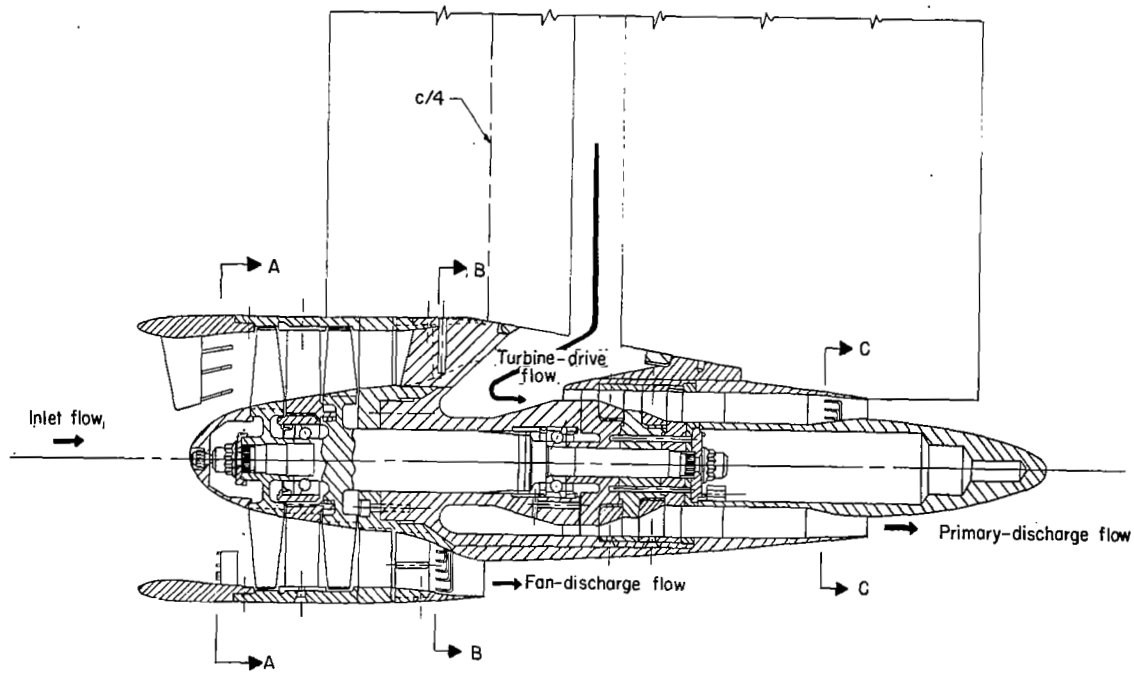
Total-pressure-rake locations

Section A-A

Section B-B
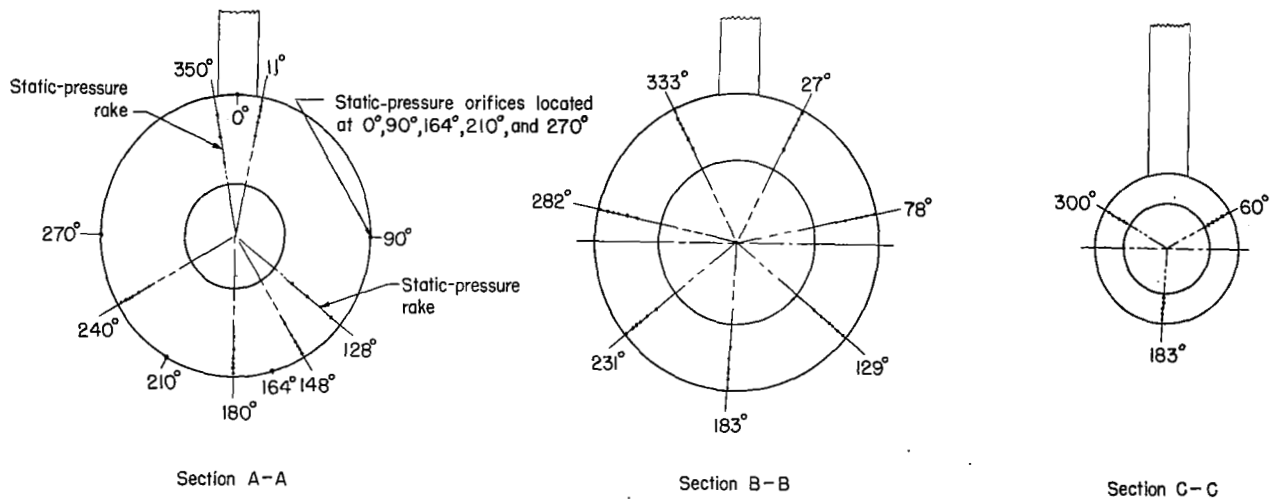
Section C-C

Figure 4.- Cross-sectional view of model fan-jet engine.
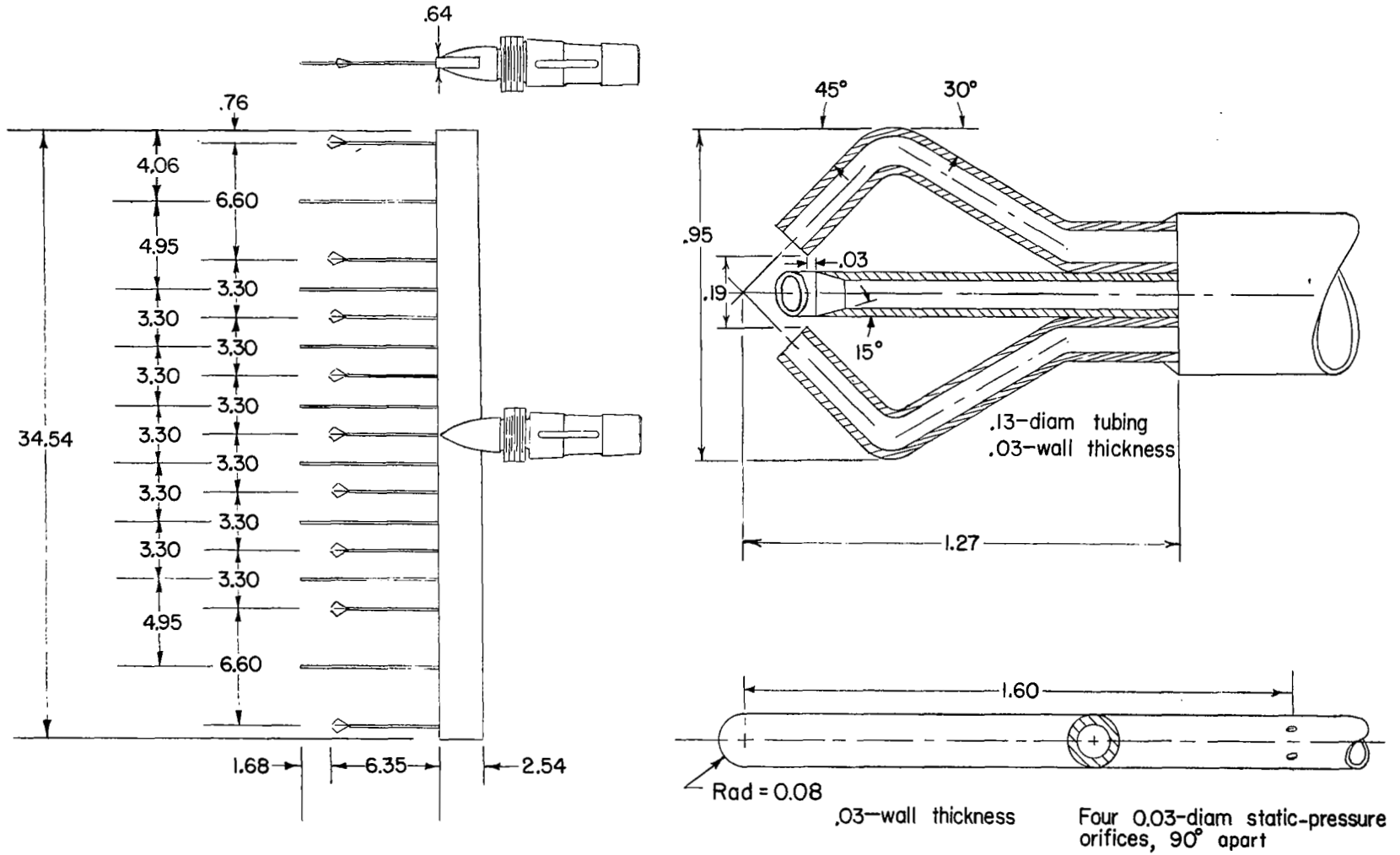
Figure 5.- Drawing of yaw rake. All dimensions are in centimeters.
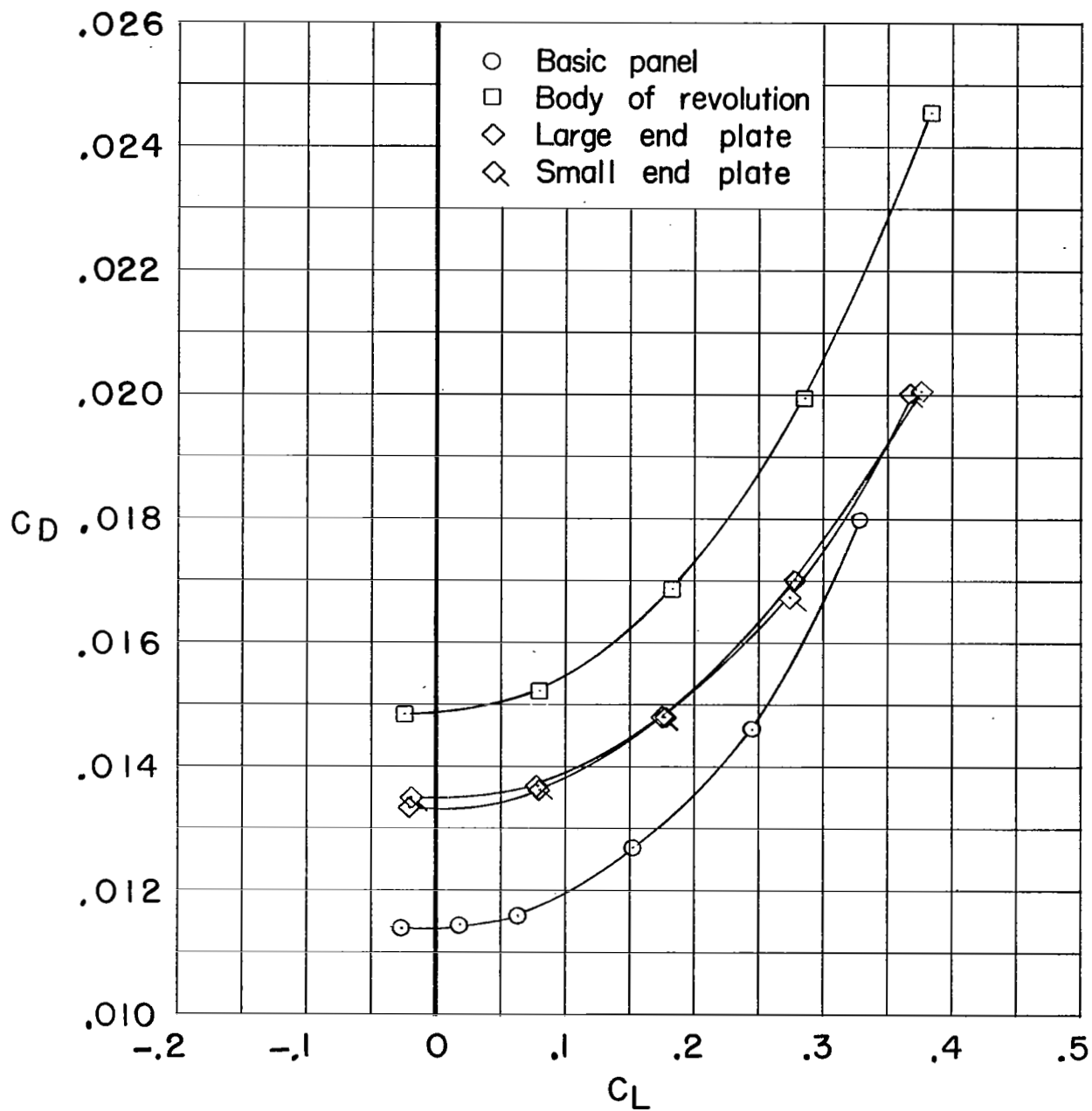
(a) C_D against C_L for basic-panel, body-of-revolution, and end-plate configurations.

Figure 6.- Basic aerodynamic characteristics of various panel-tip configurations.
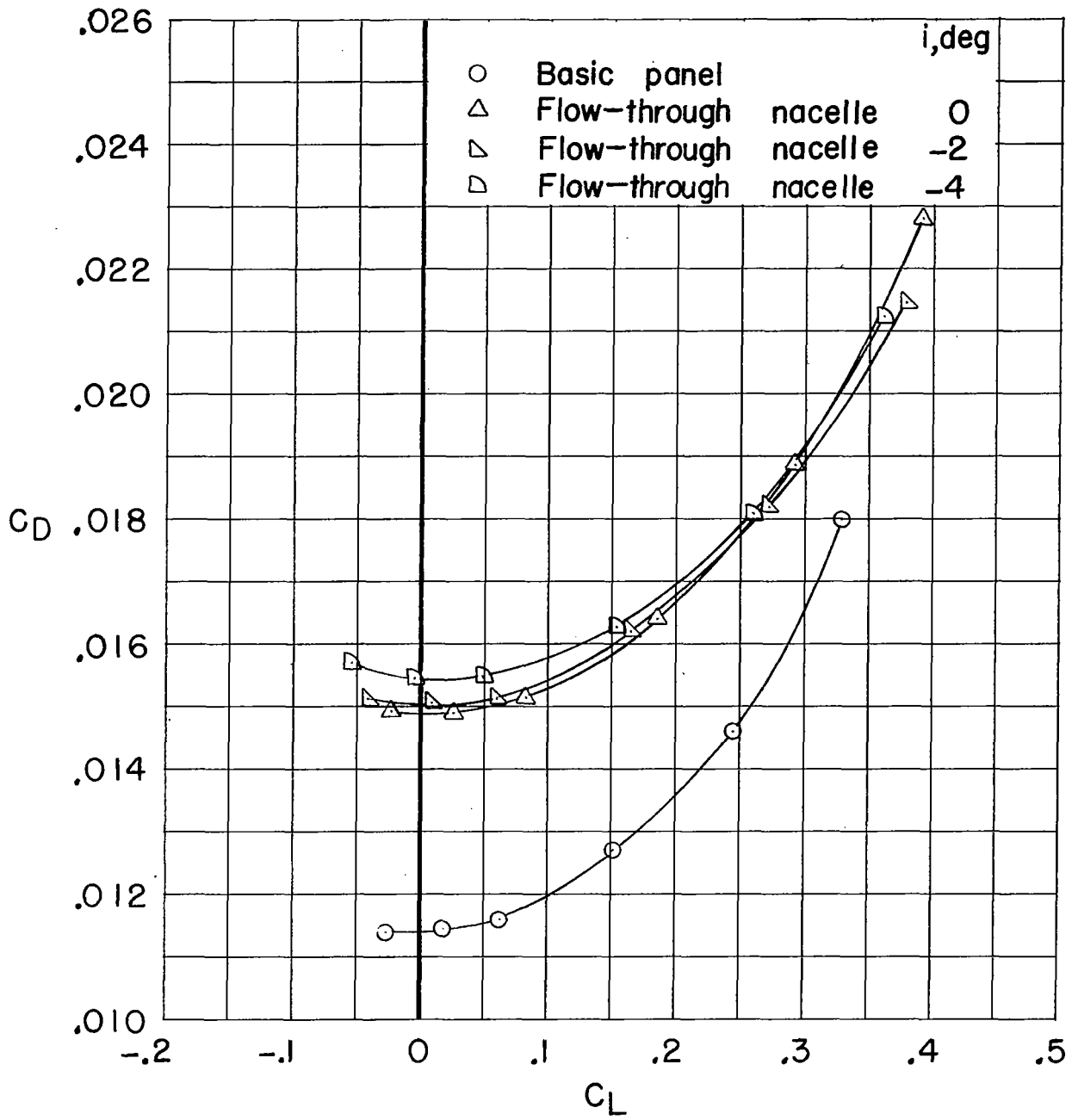
(b) C_D against C_L for basic panel and tip-mounted flow-through nacelle.

Figure 6.- Continued.
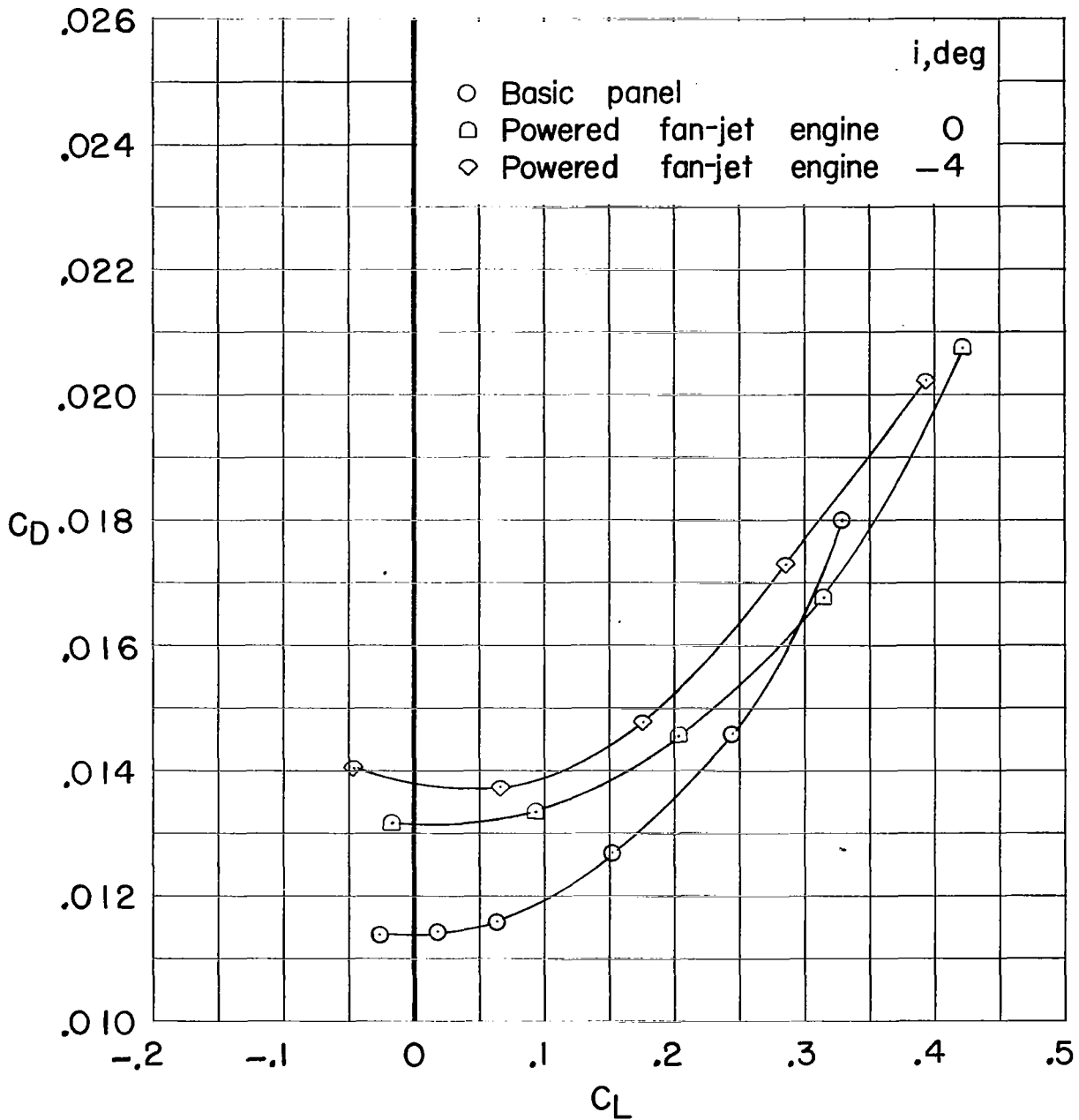
(c) C_D against C_L for basic panel and tip-mounted powered engine (maximum rpm).
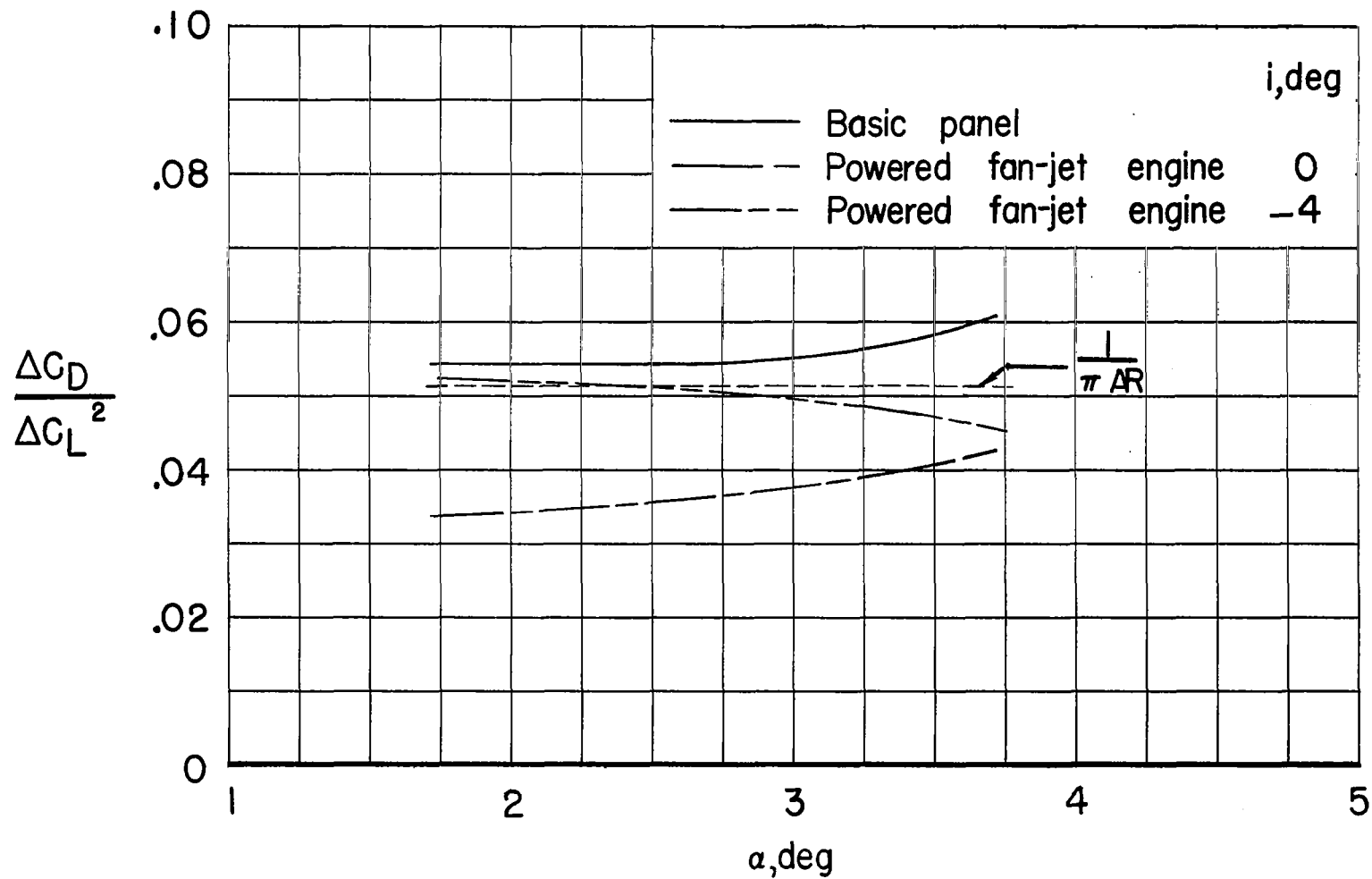
Figure 6.- Concluded.
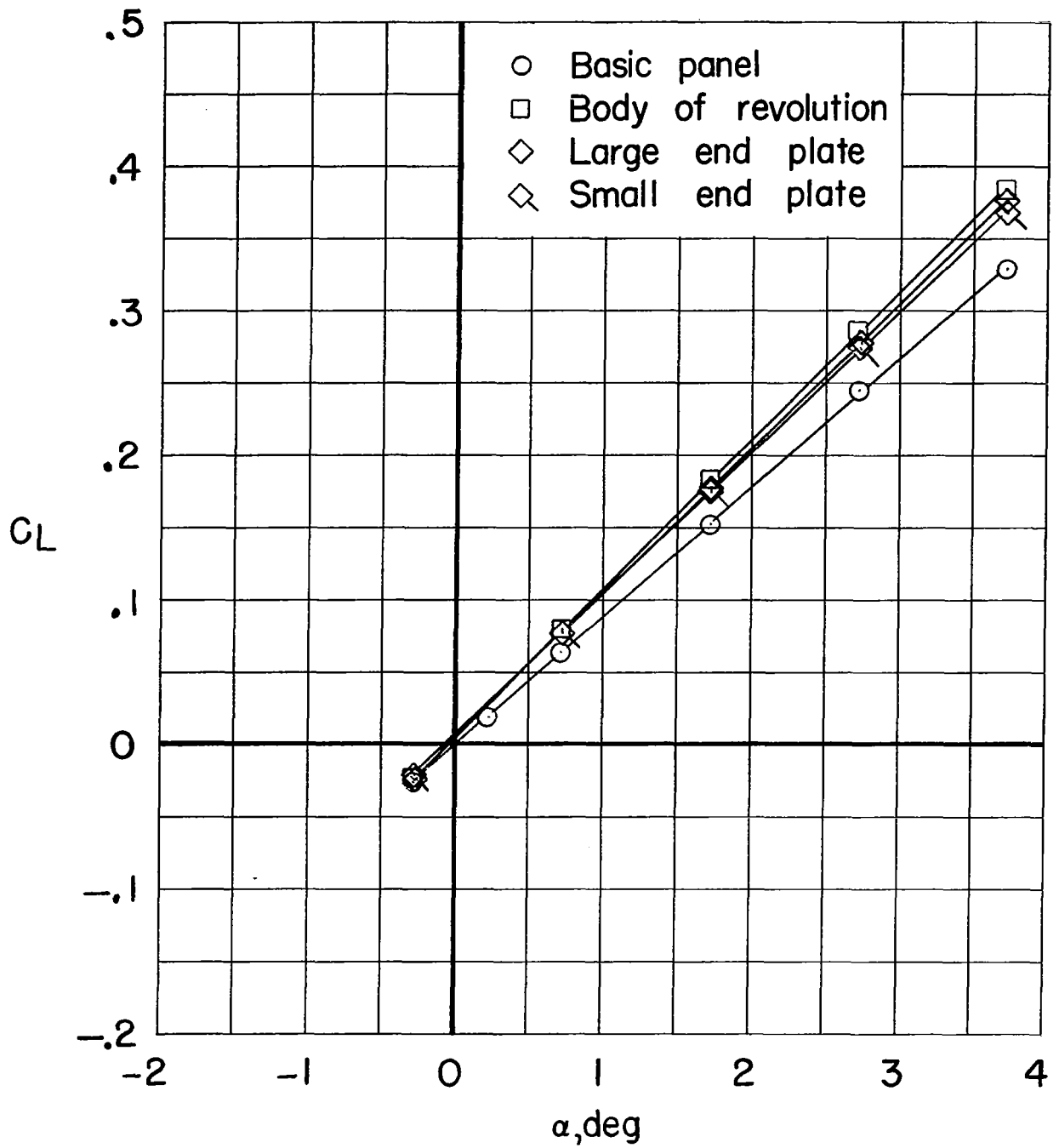
(a) C_L against α for basic-panel, body-of-revolution, and end-plate configurations.

Figure 7.- Basic aerodynamic characteristics of various panel-tip configurations.
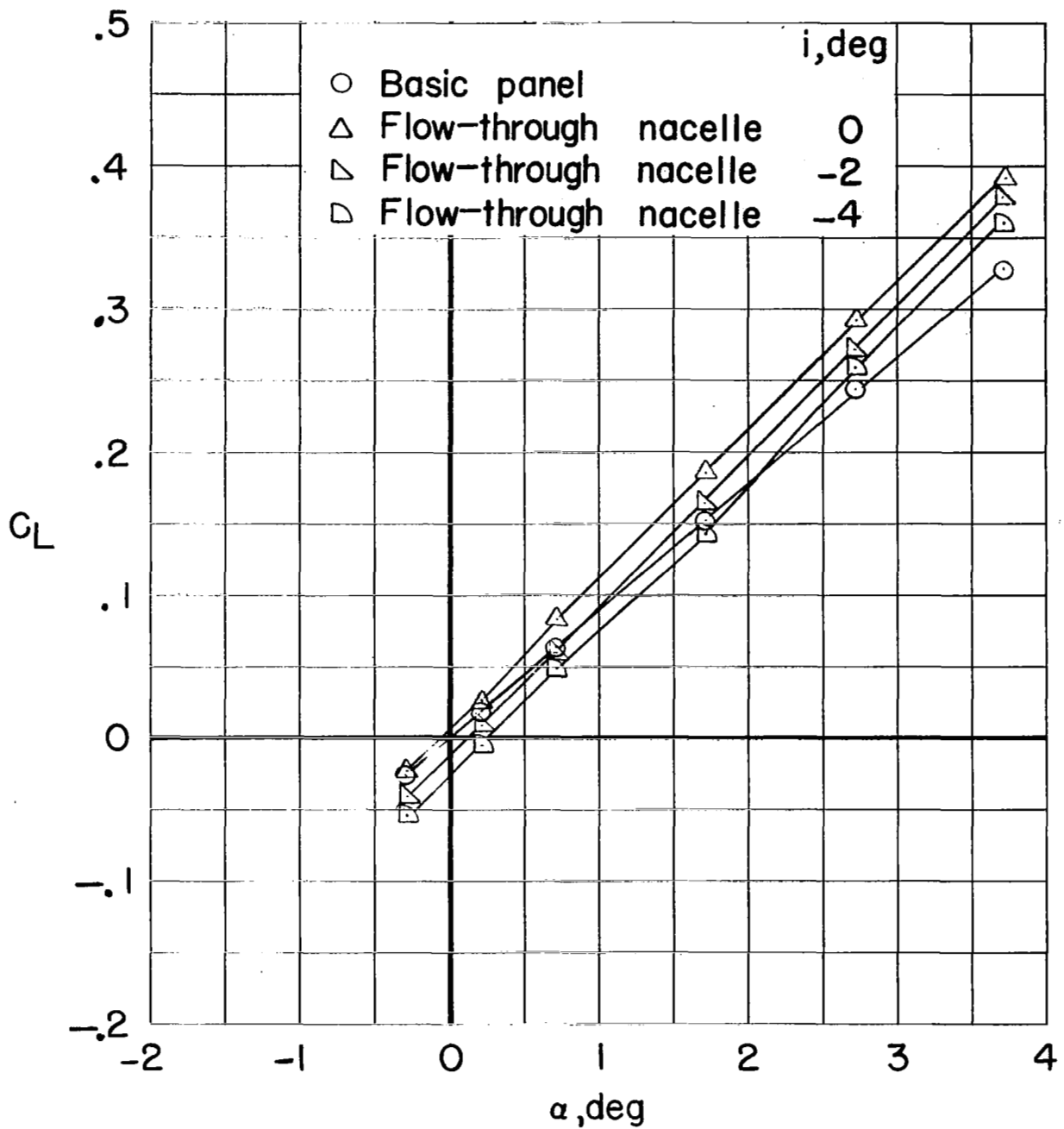
(b) C_L against α for basic panel and tip-mounted flow-through nacelle.

Figure 7.- Continued.
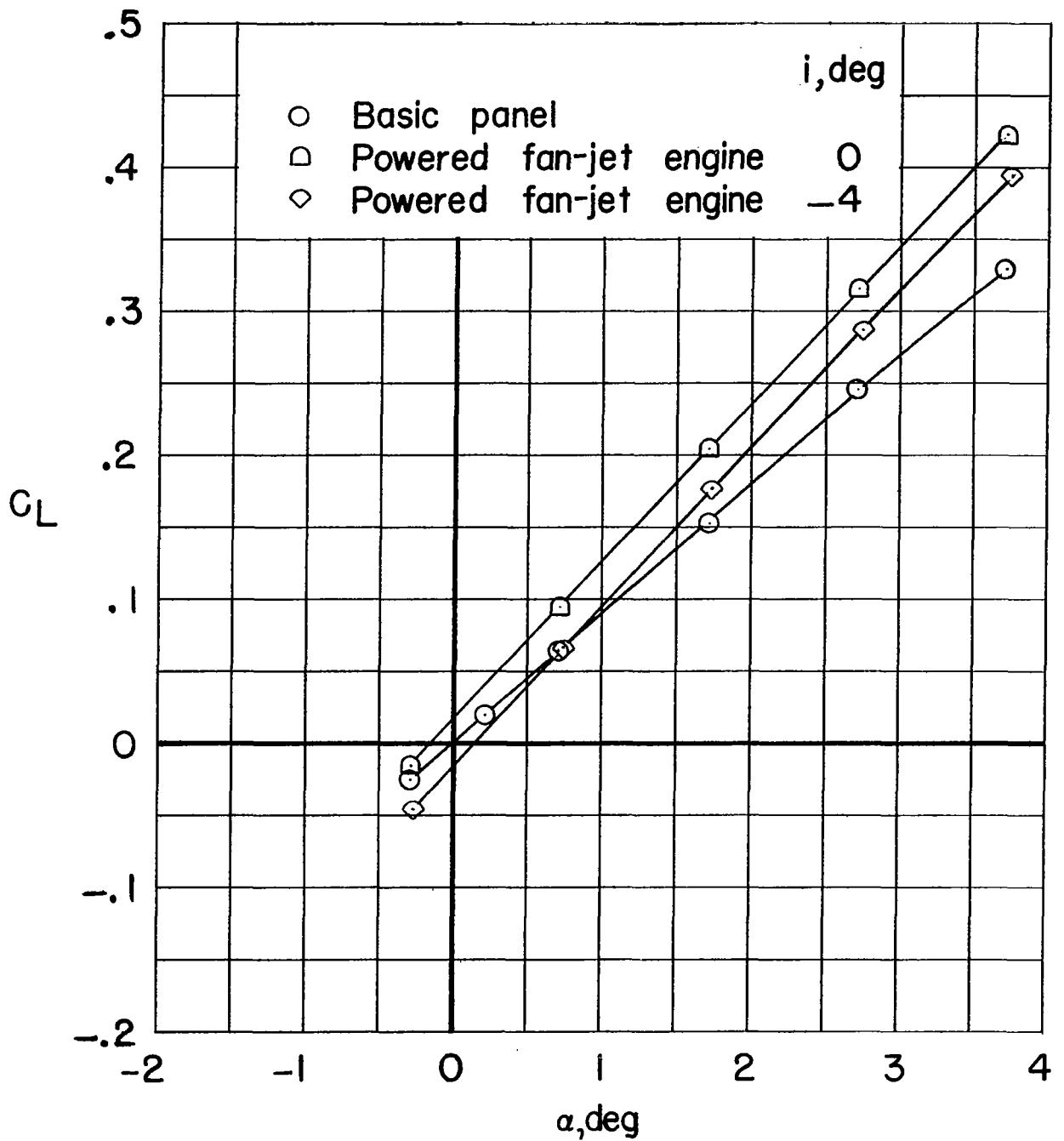
(c) C_L against α for basic panel and tip-mounted powered engine (maximum rpm).

Figure 7.- Concluded.
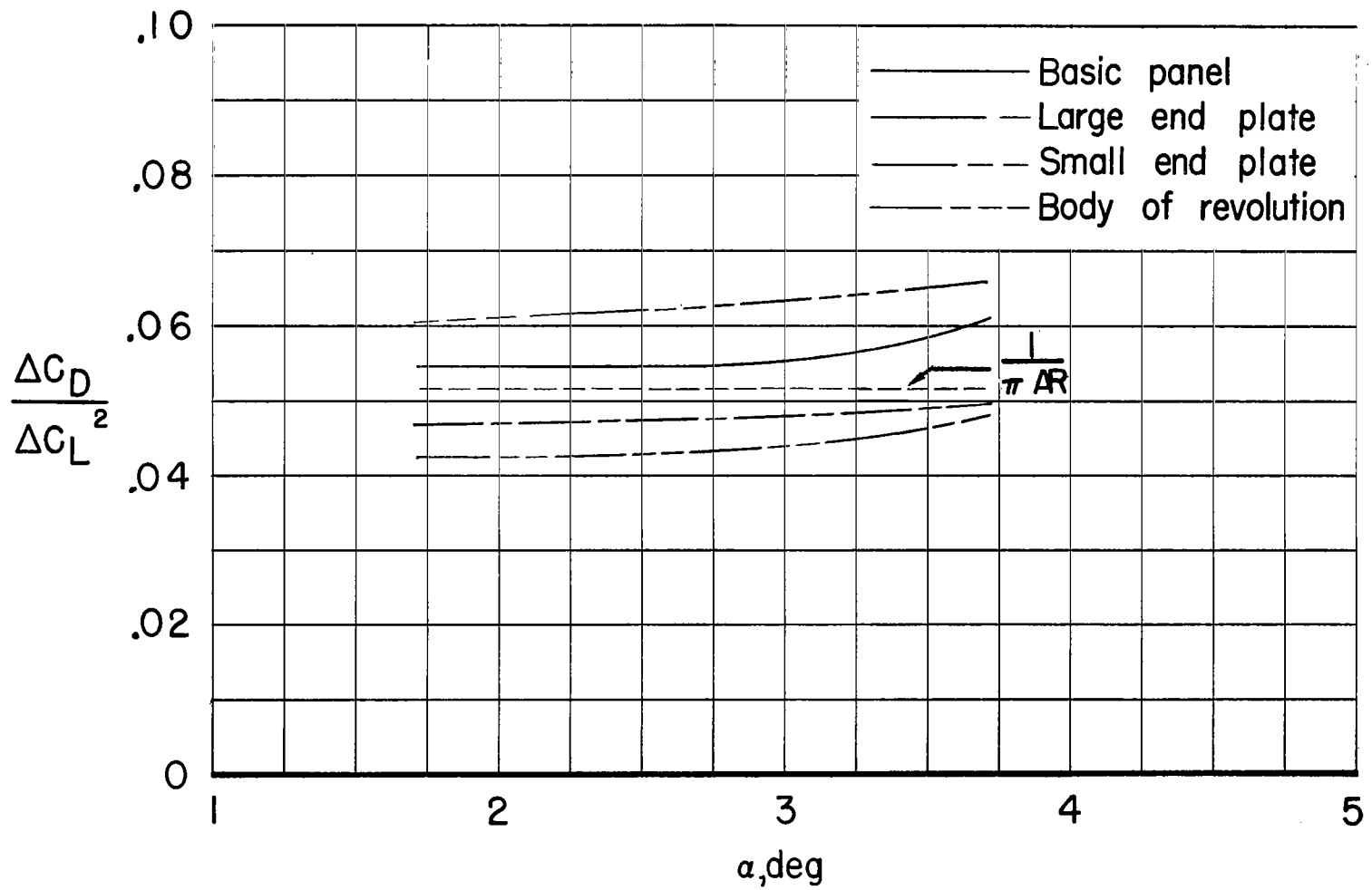
(a) $\dfrac{\Delta C_D}{\Delta C_L{}^2}$ against α for basic-panel, body-of-revolution, and end-plate configurations.

Figure 8.- Variation of drag due to lift with angle of attack for various panel-tip configurations.
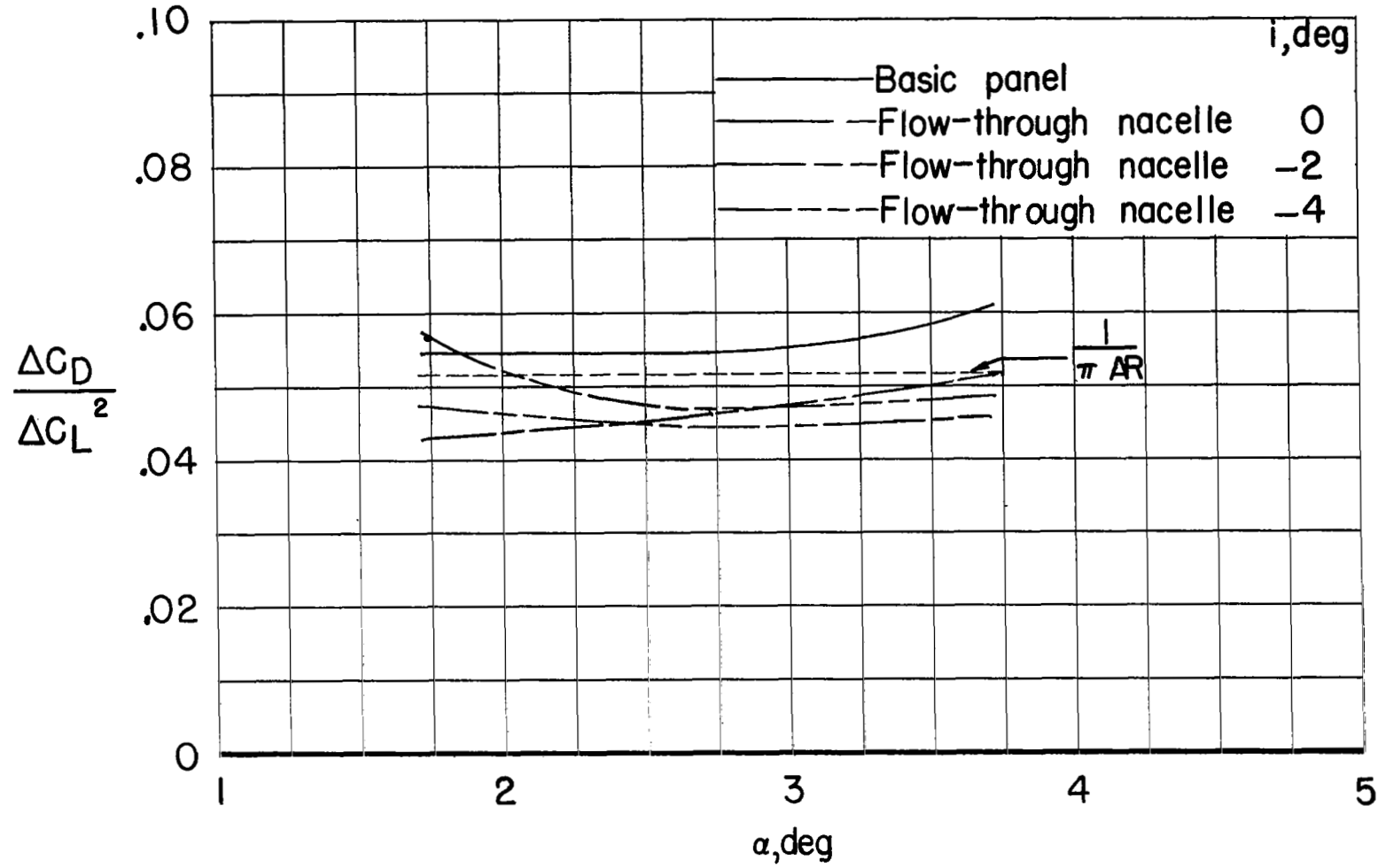
(b) $\dfrac{\Delta C_D}{\Delta C_L{}^2}$ against α for basic panel and flow-through nacelle.

Figure 8.- Continued.

(c) $\frac{\Delta C_D}{\Delta C_L^2}$ presented against α for basic panel and powered engine (maximum rpm).
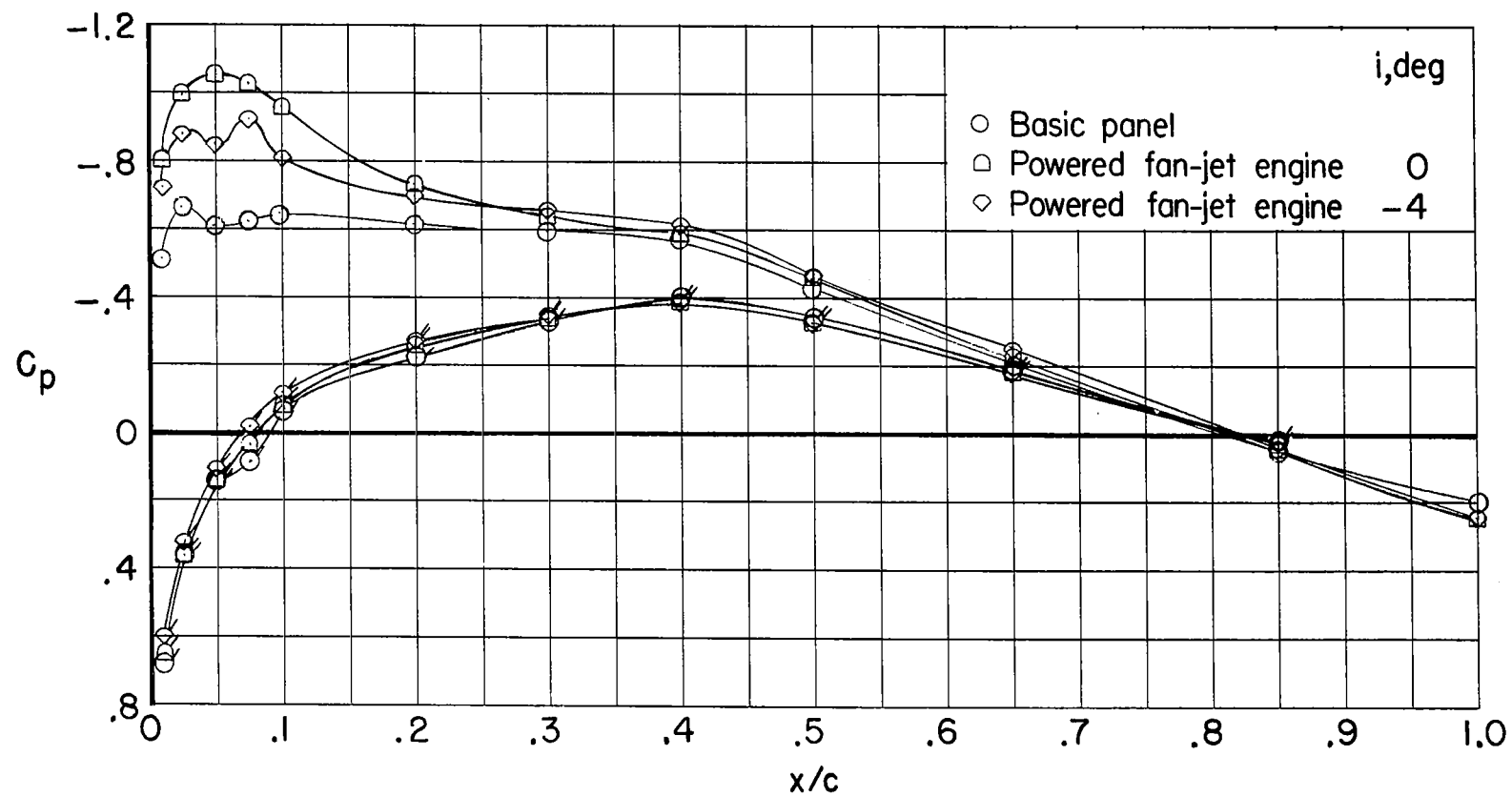
Figure 8.- Concluded.
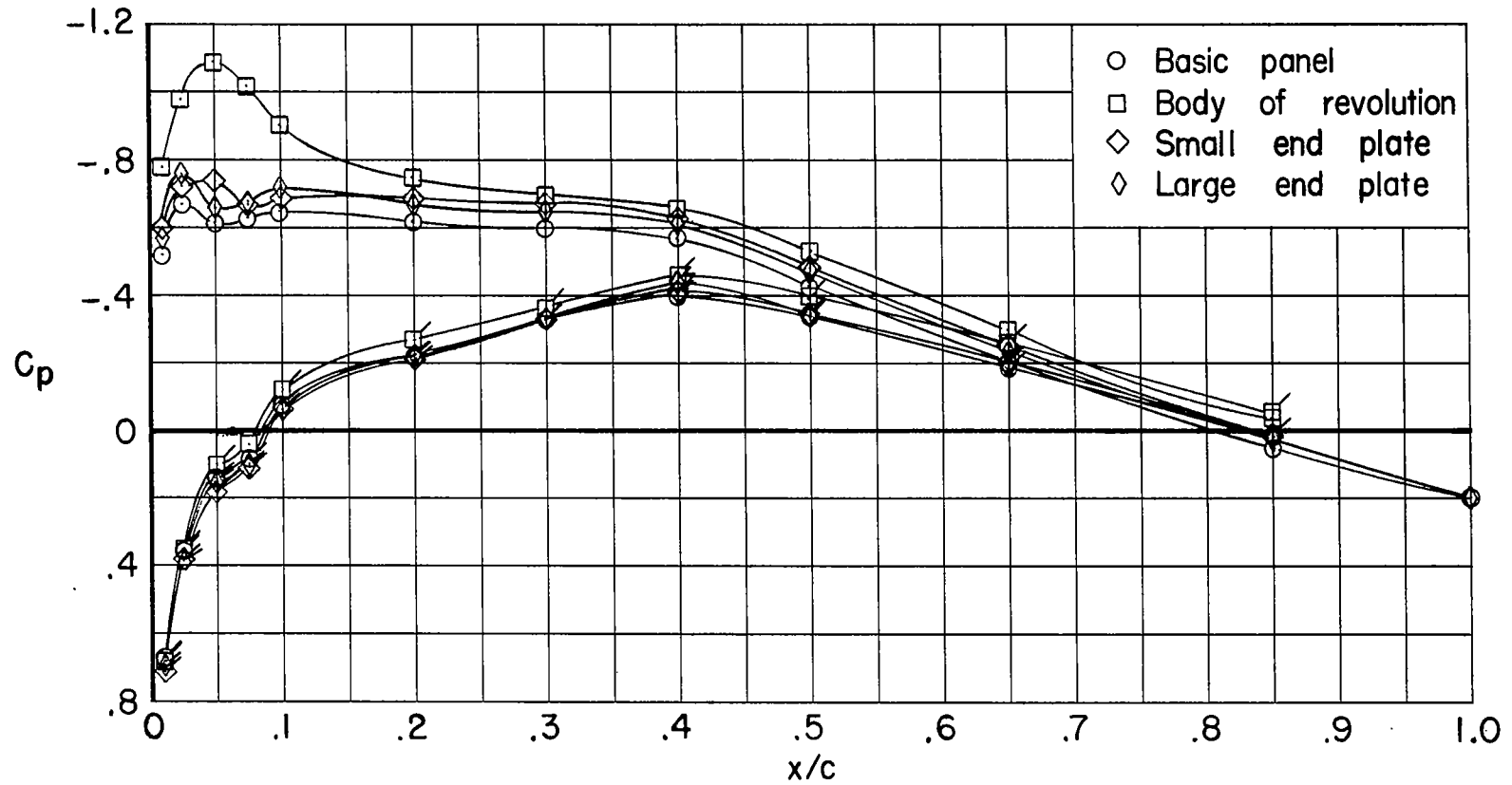
(a) Wing pressures against percent chord for basic panel, body of revolution, large end plate, and small end plate.

Figure 9.- Wing pressure distribution for various tip configurations measured at 87-percent-span location. M = 0.70; α ≈ 2.7°; flagged symbols indicate lower surface.
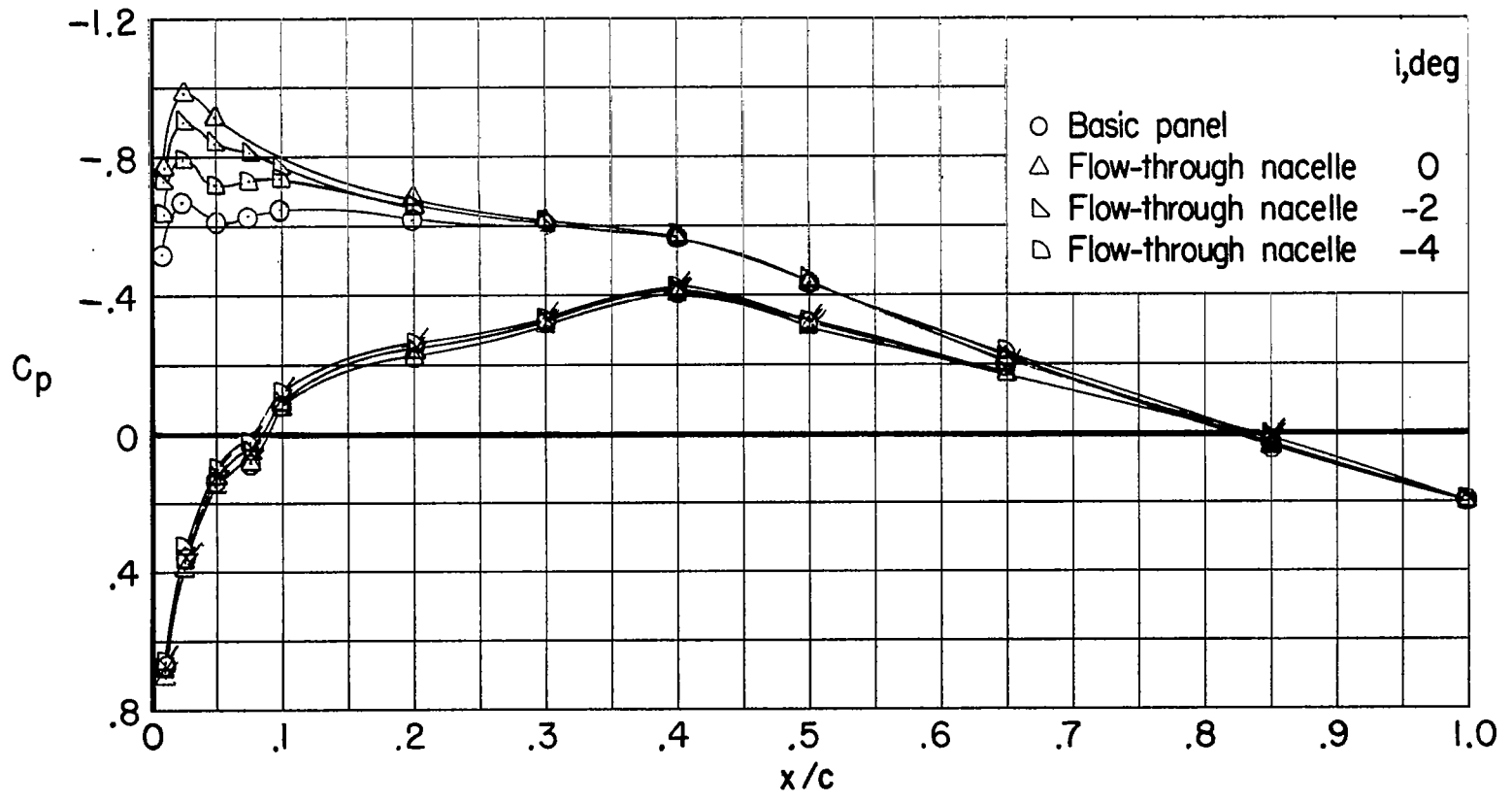
(b) Wing pressures against percent chord for basic panel and flow-through nacelle.

Figure 9.- Continued.

(c) Wing pressures against percent chord for basic panel and powered engine (maximum rpm).
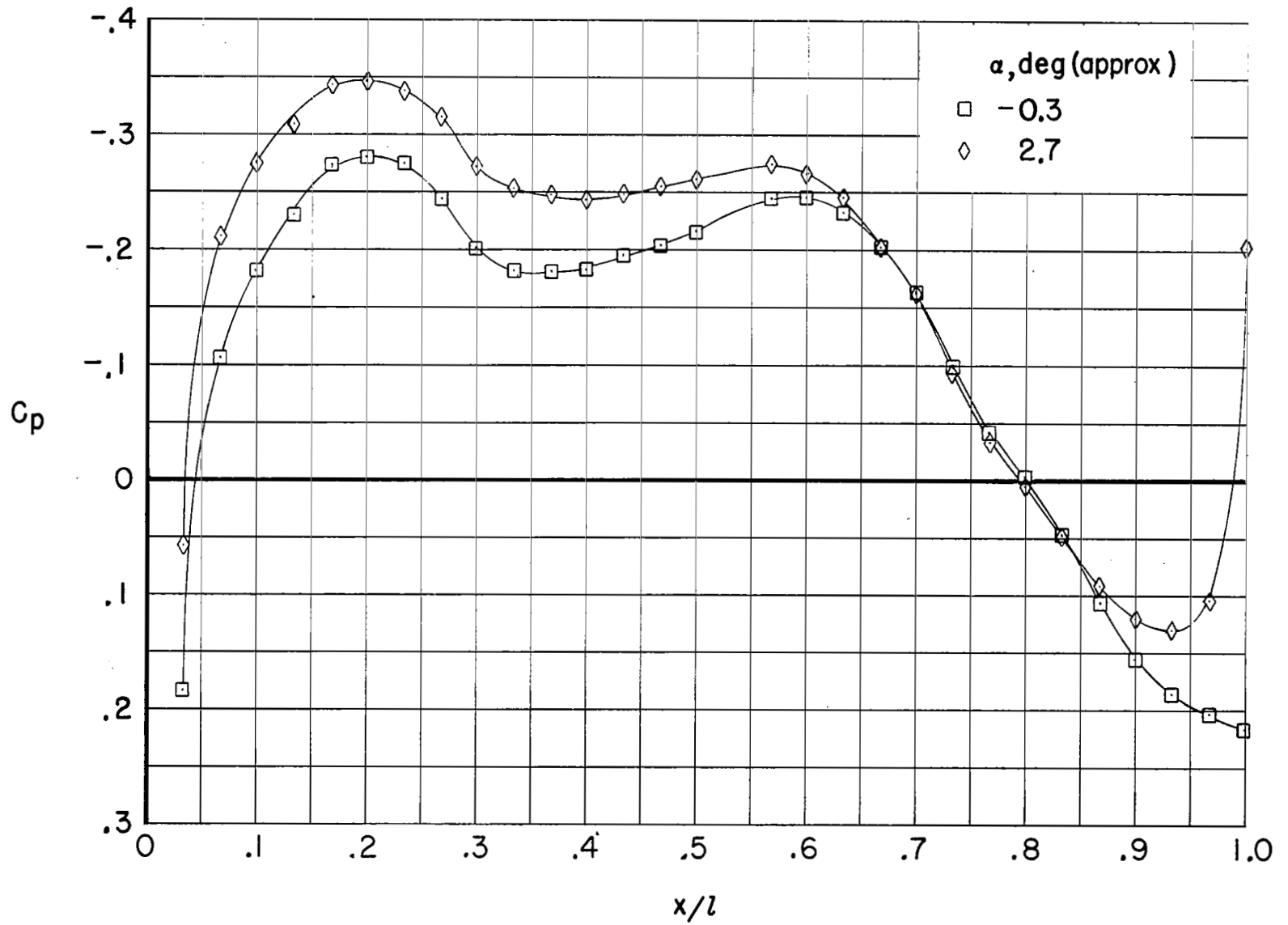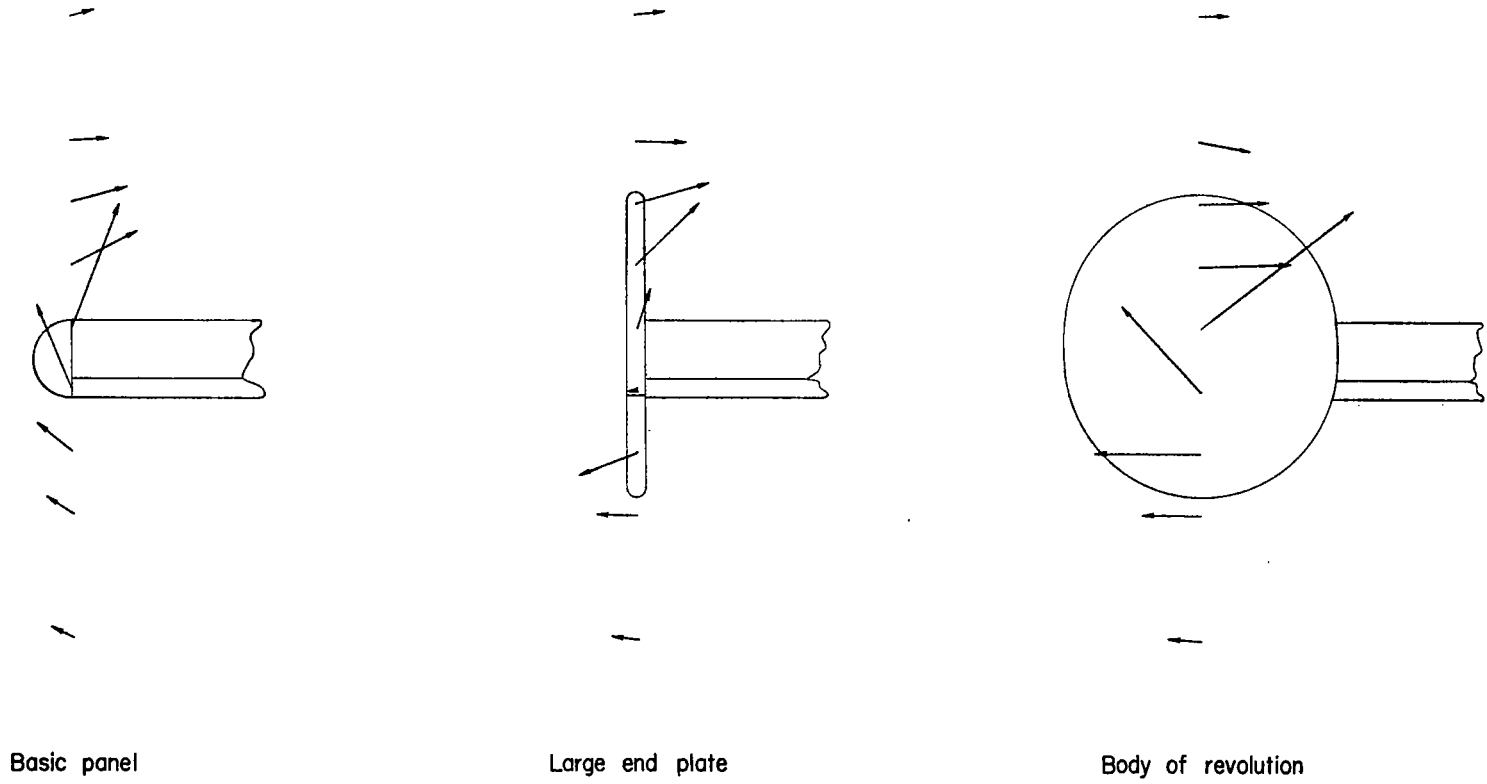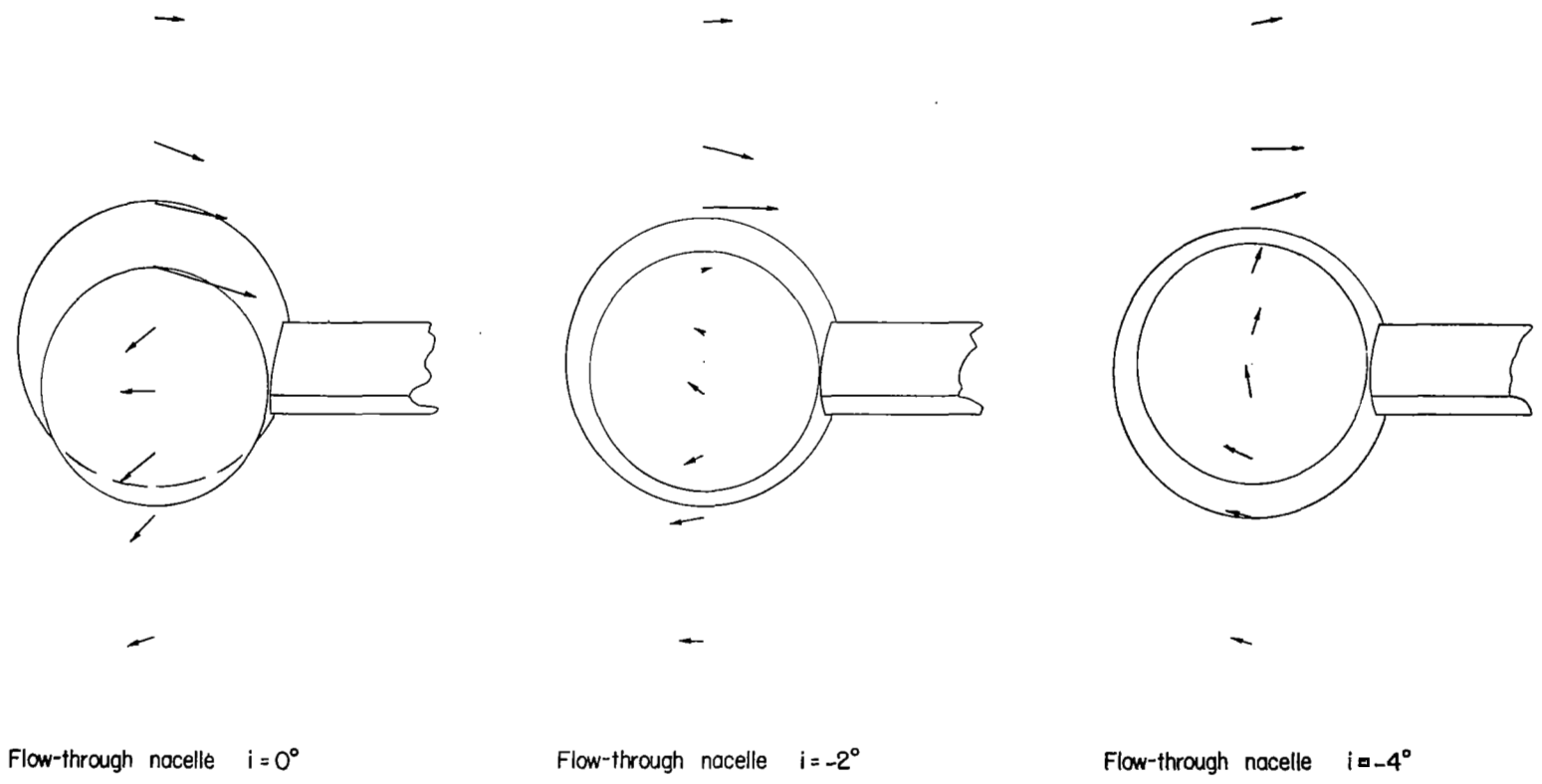
Figure 9.- Concluded.

Figure 10.- Pressure distribution along upper center line of body of revolution.

Basic panel

Large end plate

Body of revolution

(a) Vortex velocity vectors for basic panel, large end plate, and body of revolution.

Figure 11.- Tip-vortex velocity profile measured 1.5-chord length downstream of 50-percent-chord location.

Flow-through nacelle   i = 0°

Flow-through nacelle   i = -2°

Flow-through nacelle   i = -4°

(b) Vortex velocity vectors for flow-through nacelle at nacelle incidence angles of 0°, -2°, and -4°.

Figure 11.- Concluded.

"The aeronautical and space activities of the United States shall be conducted so as to contribute . . . to the expansion of human knowledge of phenomena in the atmosphere and space. The Administration shall provide for the widest practicable and appropriate dissemination of information concerning its activities and the results thereof."

— NATIONAL AERONAUTICS AND SPACE ACT OF 1958

NASA SCIENTIFIC AND TECHNICAL PUBLICATIONS

TECHNICAL REPORTS: Scientific and technical information considered important, complete, and a lasting contribution to existing knowledge.

TECHNICAL NOTES: Information less broad in scope but nevertheless of importance as a contribution to existing knowledge.

TECHNICAL MEMORANDUMS: Information receiving limited distribution because of preliminary data, security classification, or other reasons.

CONTRACTOR REPORTS: Scientific and technical information generated under a NASA contract or grant and considered an important contribution to existing knowledge.

TECHNICAL TRANSLATIONS: Information published in a foreign language considered to merit NASA distribution in English.

SPECIAL PUBLICATIONS: Information derived from or of value to NASA activities. Publications include conference proceedings, monographs, data compilations, handbooks, sourcebooks, and special bibliographies.

TECHNOLOGY UTILIZATION PUBLICATIONS: Information on technology used by NASA that may be of particular interest in commercial and other non-aerospace applications. Publications include Tech Briefs, Technology Utilization Reports and Notes, and Technology Surveys.

Details on the availability of these publications may be obtained from:

SCIENTIFIC AND TECHNICAL INFORMATION DIVISION

NATIONAL AERONAUTICS AND SPACE ADMINISTRATION
Washington, D.C. 20546